Perspective

Smart Molecular Imaging and Theranostic Probes by Enzymatic Molecular In Situ Self-Assembly

Xidan Wen,[#] Chao Zhang,[#] Yuyang Tian, Yinxing Miao, Shaohai Liu, Jing-Juan Xu, Deju Ye,* and Jian He*

Cite This: JACS Au 2024, 4, 2426−2450

Read Online

ACCESS | Metrics & More | Article Recommendations

ABSTRACT: Enzymatic molecular in situ self-assembly (E-MISA) that enables the synthesis of high-order nanostructures from synthetic small molecules inside a living subject has emerged as a promising strategy for molecular imaging and theranostics. This strategy leverages the catalytic activity of an enzyme to trigger probe substrate conversion and assembly in situ, permitting prolonging retention and congregating many molecules of probes in the targeted cells or tissues. Enhanced imaging signals or therapeutic functions can be achieved by responding to a specific enzyme. This E-MISA strategy has been successfully applied for the development of enzyme-activated smart molecular imaging or theranostic probes for in vivo applications. In this Perspective, we discuss the general principle of controlling in situ self-assembly of synthetic small molecules by an enzyme and then discuss the applications for the construction of "smart" imaging and theranostic probes against cancers and bacteria. Finally, we discuss the current challenges and perspectives in utilizing the E-MISA strategy for disease diagnoses and therapies, particularly for clinical translation.

KEYWORDS: molecular imaging, in situ self-assembly, theranostics, enzyme, in vivo
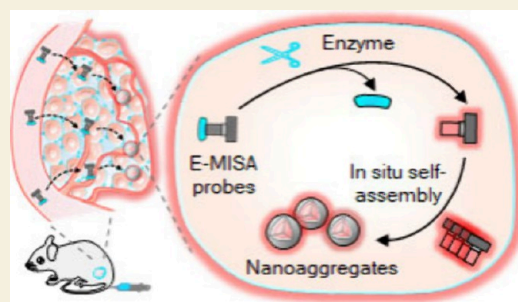
1. INTRODUCTION

Self-assembly of small molecules into intricate, high-order functional nanostructures is a ubiquitous phenomenon in nature, participating in many important physiological and pathological processes.[1−4] Inspired by this, extensive efforts have been made to harness the self-assembly process to control the synthesis of nano/microstructures in either solutions or living subjects.[5,6] In particular, the stimuli-triggered molecular in situ self-assembly strategy, which enables the on-site synthesis of nanostructures from synthetic small molecules within living organisms, has found a wide range of applications in biology and medicine. These include tissue engineering, controlled drug delivery, regulation of cellular functions, molecular imaging, and so forth.[7−13] This approach diverges from conventional small-molecule therapeutics and nanomaterials by employing small-molecule probes that can be specifically recognized or activated by a stimulus. Activation induces a transformation in the molecular structure of the probes from hydrophilic to amphiphilic (or hydrophobic), which in turn drives self-assembly at the site of action through molecular interactions. These forces, including $\pi−\pi$ stacking,[14,15] hydrophobic interactions,[16,17] hydrogen bonding,[18,19] electrostatic interactions,[20] coordination bonds,[21] etc.,[22,23] facilitate the in situ formation of nanostructures with improved retention and accumulation at the target site. The stimuli-responsive in situ self-assembly strategy offers several

advantages over traditional therapeutic modalities.[24−26] It mitigates the rapid clearance from the target area that is typical for small molecules and addresses the challenges of high reticuloendothelial system (RES) uptake as well as limited penetration associated with nanomaterials in vivo.[27−30] By combining the inherent high tissue penetration of small molecules (before activation) with the prolonged retention of nanomaterials (postactivation), this strategy can significantly enhance accumulation and retention of molecular probes at the targeted tissues. Thus, enhanced imaging signals and/or therapeutic activities can be achieved in the target tissues, while inactivated small-molecule probes can be easily washed out of from nontarget normal tissues, which is beneficial to reduce background signals and/or side effects in vivo.[31,32]
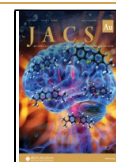
In recent years, numerous molecular probes have been developed for the imaging and/or treatment of tumors or other diseases in vivo based on the stimuli-triggered molecular in situ self-assembly strategy.[33−35] These self-assembly molecular probes can be responsive to different stimuli, such as
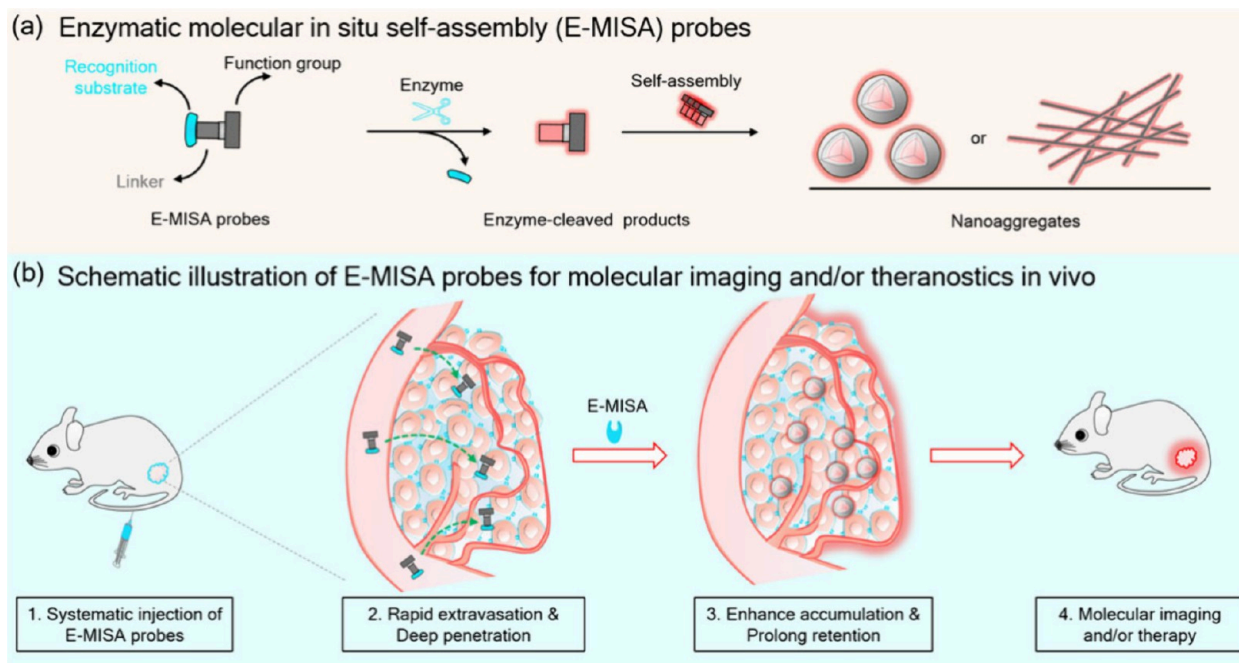
Figure 1. Schematic illustration of enzymatic molecular in situ self-assembly (E-MISA) probes for in vivo imaging and/or theranostics. (a) Design of E-MISA probes and proposed enzyme-triggered self-assembly process. (b) Schematic illustration of E-MISA probes for molecular imaging and/or theranostics in vivo.

pH,[36,37] reactive oxygen species (ROS),[38,39] biothiols,[40,41] light,[42,43] temperature,[44,45] ultrasound (US),[46,47] enzymes,[48,49] antigens,[50,51] and nucleic acids.[52,53] Among these stimuli, enzymes represent a type of important molecular triggers due to their crucial roles in controlling various biological processes.[54−57] It has been recognized that aberrant expression of enzymes is intricately linked to metabolic disorders, genetic diseases, and impaired physiological functions. Precise in vivo detection of their activity is significant for the diagnosis of tumors and other diseases.[58−66] The enzymatic molecular in situ self-assembly (E-MISA) strategy has shown promise for molecular imaging and theranostics.[67] Unlike the other approaches for the imaging of enzymes, the E-MISA strategy utilizes the catalytic activity of an enzyme under mild physiological conditions, which allows catalysis of the continuous conversion of a hydrophilic small-molecule precursor into the amphiphilic (or hydrophobic) intermediates near the site of the targeted enzyme. As a result, the local concentration of the intermediates is above the critical micelle concentration (CMC), permitting triggering of efficient molecular self-assembly into nanoaggregates.[68] This process facilitates the accumulation of many self-assembly probes in the target tissues for improving imaging and/or therapy of diseases.[69] There have been some reviews to describe the enzyme-triggered molecular probes for molecular imaging and/or theranostics of tumors.[26,39,70−72] However, there is still a lack of a comprehensive perspective to provide a systematic and timely summary of the progress in E-MISA probes for in vivo imaging of enzymatic activity and for controlled drug release for cancer theranostics.

In this Perspective, we provide an overview of the E-MISA strategy for the design of smart molecular probes for in vivo imaging and theranostics. We briefly introduce the general strategy for the design of E-MISA probes, which include monomodality imaging probes, multimodality imaging probes, and multifunctional theranostics probes. We then discuss the applications of these E-MISA probes for in vivo imaging and theranostics of tumors and other diseases. Finally, current challenges and perspectives in the development of E-MISA probes for disease diagnoses, therapies, and clinical translation are discussed.

2. GENERAL STRATEGIES FOR THE DESIGN OF E-MISA PROBES

Figure 1a illustrates the general components of an E-MISA probe, which consists of (1) an enzyme recognition substrate, (2) a linker to promote self-assembly,[73,74] and (3) a function group for imaging and/or therapy. The E-MISA probe is typically designed to be water-soluble initially. After cleavage by the target enzyme, it undergoes molecular transformation to generate the amphiphilic (or hydrophobic) product, which subsequently proceeds with molecular self-assembly into nanoaggregates (e.g., nanoparticles and nanofibers). The applications of the E-MISA probes for in vivo imaging and/or therapy are illustrated in Figure 1b. After systemic injection, they can easily extravasate and penetrate into biological tissues due to their small size and hydrophilicity. In the target tissues where the enzymes of interest are present, they can proceed via an on-demand E-MISA process, affording nanoaggregates with significantly increased molecular size. This can help to enhance accumulation and retention at the target tissues, leading to increased imaging contrast and therapeutic efficacy in vivo. To enable the E-MISA strategy, it is important to choose the target enzyme. Ideally, the target enzyme should be overexpressed in the targeted tissue but have low (or no) expression in the nontargeted tissues. The target enzyme can potentially act as a biomarker of a disease (e.g., cancer, bacteria). Additionally, the target enzyme should have a high catalytic activity and specificity.[75] In recent years, people have developed a number of E-MISA probes that are responsive to either extracellular enzymes (e.g., metalloproteinases
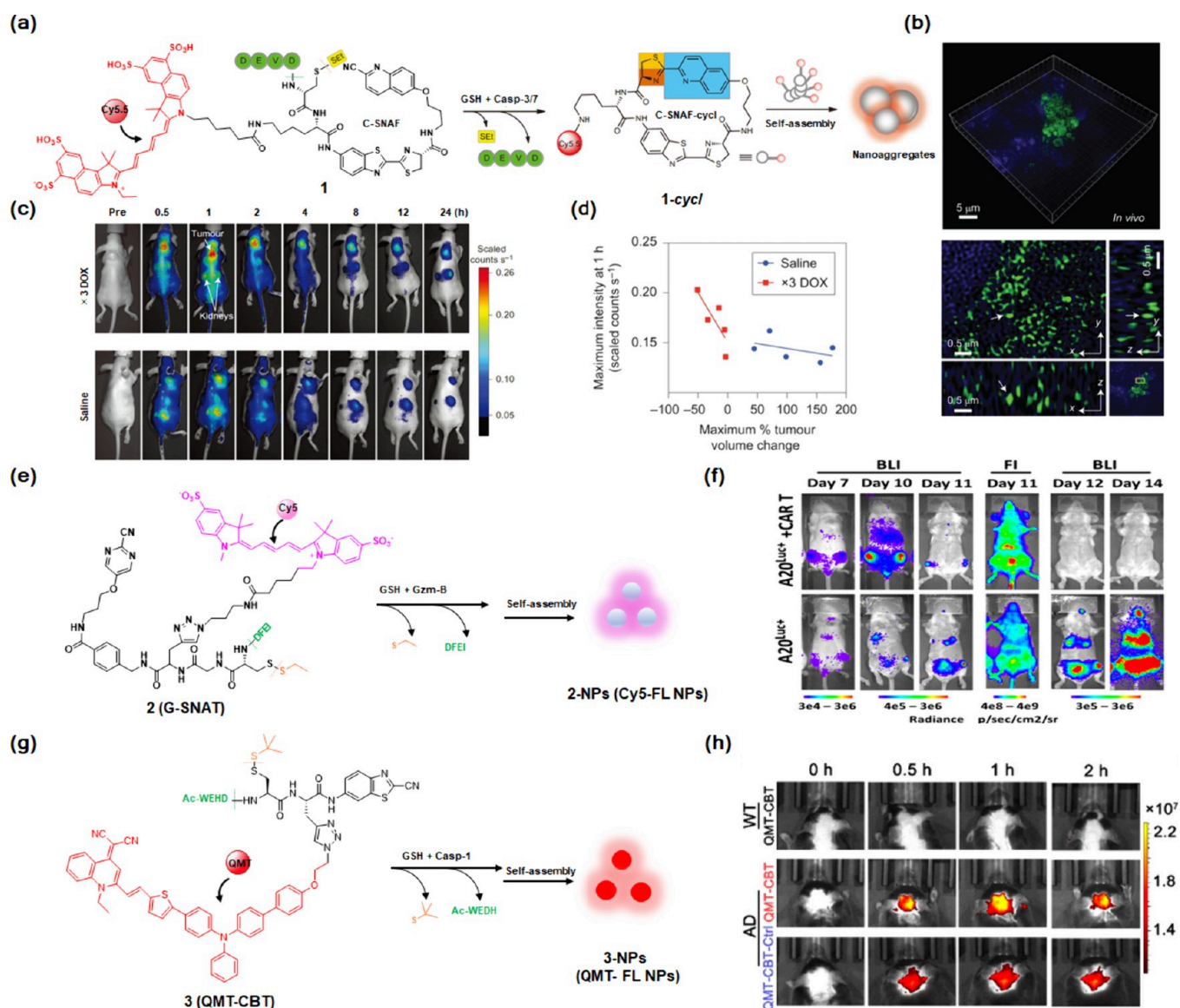
Figure 2. E-MISA fluorescent probes and their chemical structures. (a) Chemical structure of probe **1** and the proposed chemical conversion in the presence of GSH and casp-3/7. (b) (top) Representative three-dimensional structured illumination microscopy (3D-SIM) image of a DOX-treated tumor tissue slice from HeLa tumor-bearing mice after intravenous (i.v.) injection of probe **1** (pseudo-green) and (bottom) the enlarged area of interest region in the 3D-SIM image. The cell nuclei are costained with DAPI (blue). (c) Longitudinal fluorescence imaging (FLI) of HeLa tumor-bearing mice treated with DOX or saline after intravenous injection of probe **1**. (d) Plots of the maximum tumor FL intensity at 1 h after i.v. injection of probe **1** versus the maximum % tumor volume change after ×3 DOX-treated (red, Pearson's $r = -0.9$, $P < 0.05$) or saline-treated mice (blue, $r = -0.2$, $P > 0.05$). (e) Chemical structure of probe **2** and its conversion to NIR fluorescent **2**-NPs via the E-MISA process in the presence of Gzm-B and GSH. (f) Longitudinal bioluminescence imaging (BLI), and FLI with D-luciferin and probe **2** (5 nmol, ex 650 nm/em 670 nm) of (bottom) A20^{Luc+}-implanted or (top) CAR T cell-treated tumor-bearing mice. (g) Chemical structure and the proposed chemical conversion mechanism of E-MISA fluorescent probe **3** (QMT-CBT). (h) Fluorescence images of WT and AD mice preinjected with cyclosporin (0.04 mg kg^{-1}) for 1 h, followed by i.v. injection of **3** or QMT-CBT-Ctrl (0.2 mg kg^{-1}). Reproduced with permission from ref 96 (copyright 2014 Springer Nature), ref 125 (CC BY-NC-ND 4.0), and 128 (copyright 2023 American Chemical Society).

(MMPs),[76−78] alkaline phosphatase (ALP),[79−90] γ-glutamyl transferase (GGT)[91,92] or intracellular enzymes (e.g., furin,[93−95] caspase3/7 (casp-3/7),[96−108] cathepsin B (cat B),[109−111] β-galactosidase (β-gal),[112] etc.)[113] of cancer or disease-relevant cells. These E-MISA probes can leverage the enzymatic catalysis to control proteolysis and self-assembly of many molecules of probes, which are beneficial to amplify imaging signals or increase therapeutic outcomes in tumors or related diseases.

According to the enzymatic functions, two general strategies are commonly employed to control probe self-assembly. First,

enzyme-triggered proteolysis manipulates direct molecular self-assembly. Second, enzyme-triggered biocompatible reaction that manipulates molecular self-assembly. With the introduction of various imaging moieties, E-MISA probes with different imaging modalities can be designed.[114,115] By introducing different therapeutic groups, it is feasible to construct therapeutic E-MISA probes for chemotherapy, phototherapy, sonodynamic therapy (SDT), and combination therapy. Furthermore, theranostic E-MISA probes can also be designed by integrating both imaging and therapeutic components. In the following sections, we first discuss the progress of E-MISA

probes in in vivo imaging, ranging from monomodality imaging to multimodality imaging. The monomodality E-MISA imaging probes mainly consist of fluorescence imaging (FLI), magnetic resonance imaging (MRI), positron emission tomography (PET), and photoacoustic imaging (PAI) probes. We then discuss the progress of E-MISA probes in theranostics, including chemotherapy, phototherapy and/or SDT, and combination therapy.

3. E-MISA PROBES FOR MOLECULAR IMAGING OF ENZYMATIC ACTIVITY

3.1. E-MISA Probes for FLI of Enzymatic Activity

FLI is a cost-effective, noninvasive, and simple technique that has been widely utilized for the sensitive detection of enzyme activity both in vitro and in vivo.[116−119] By incorporating different fluorophores into E-MISA probes, different enzyme activities can be detected by selectively controlling the self-assembly of probes near the target enzyme sites.[120−122]

In 2010, Rao and co-workers reported the use of an enzyme-triggered biocompatible reaction between 6-hydroxy-2-cyano-benzothiazole (CBT) and D-cysteine (D-Cys) to manipulate the self-assembly of small-molecule fluorescent probes in living cells.[123,124] Later, they optimized the biocompatible reaction to outcompete endogenous L-Cys for achieving the E-MISA process in an in vivo context. As a representative, they designed a near-infrared (NIR) fluorescent E-MISA probe for in vivo imaging of casp-3/7 activity (Figure 2a).[96] This NIR fluorescent probe (named C-SNAF), which is denoted as probe **1** here, consisted of three major components: (1) a biocompatible reaction pair of 2-cyano-6-hydroxyquinoline (CHQ) and a D-Cys residue linked by an amino luciferin scaffold, (2) a casp-3/7-recognition peptide substrate (DEVD) and a glutathione (GSH)-reducible disulfide cap on the N-terminus of the D-Cys residue, and (3) the NIR fluorophore Cy5.5 for FLI. Initially, probe **1** existed in a hydrophilic and small-molecule state in solution. Upon cleavage by casp-3/7 and reduction by GSH, both the DEVD peptide and the disulfide bond were removed, yielding free N-terminal D-Cys that allowed rapid intramolecular cyclization with CHQ to afford macrocyclic **1**-*cycl* (C-SNAF-*cycl*). The enhanced hydrophobicity and rigidity of these macrocyclic **1**-*cycl* molecules could facilitate their self-assembly into fluorescent nanoaggregates with a size of 174 ± 44 nm. This size of these nanoaggregates was significantly larger compared to that of probe **1** itself, which could potentially impede the diffusion process and prolong its retention time at the site.

As active casp-3/7 is positively related to cell apoptosis, these NIR fluorescent nanoaggregates formed in situ could be trapped in therapy-responsive apoptotic tumor cells, which were visualized by three-dimensional structured illumination microscopy (3D-SIM) (Figure 2b). After intravenous (i.v.) injection of probe **1** into HeLa tumor-bearing mice, they observed that the NIR FL signal in doxorubicin (DOX)-treated tumors was significantly 1.6-fold higher than that in saline-treated tumors (Figure 2c). Moreover, they found that the tumor NIR FL increased as the chemotherapy progressed from the first round (×1 DOX) to third round (×3 DOX). The maximum FL intensity correlated strongly with the tumor-size change after therapy, suggesting that probe **1** could report the degree of tumor apoptosis following chemotherapy (Figure 2d).

In addition to FLI of casp-3/7 activity using the NIR fluorescent E-MISA probe, Rao's group also developed a granzyme B (Gzm B)-responsive E-MISA probe for multi-parameter imaging of immune cell activity in tumors. Gzm B is released from cytotoxic T lymphocytes (CTLs) during granule-mediated cytotoxicity, playing a pivotal role in assessing the efficacy of CTL-mediated cancer immune therapy. The precise detection of Gzm B activity is applicable for early evaluation of the effectiveness of immune therapy. To enable sensitive imaging of Gzm B activity, they utilized an optimized biocompatible intramolecular macrocyclization reaction between pyrimidinecarbonitrile and D-Cys and developed the Gzm B-responsive E-MISA probe **2** (named G-SNAT) by introducing a Gzm B-sensitive peptide motif (IEFD) and the NIR fluorophore Cy5.[125,126] Probe **2** could be activated to undergo intramolecular cyclization in the presence of both Gzm B and GSH, followed by in situ self-assembly to form Cy5-containing NIR fluorescent nanoparticles (Figure 2e). This Gzm B-triggered E-MISA process could enhance accumulation of Cy5 fluorophores in the Gzm B-positive tumors, affording high NIR FL signals in subcutaneous (s.c.) A20 lymphoma tumors upon receiving immunotherapy with chimeric antigen receptor (CAR) T cells. Probe **2** could be employed to permit precise detection of Gzm B activity in the CAR T-treated A20 lymphoma tumors after i.v. injection into mice, which could be utilized to monitor the efficacy of immunotherapy in tumors with immune checkpoint blockade and CAR-T in vivo (Figure 2f).

In addition, an NIR fluorescent E-MISA probe also can be utilized for Alzheimer's disease (AD) imaging. AD is a progressive neurodegenerative disorder that typically presents with neuroinflammation. Within this neuroinflammatory context of AD, caspase-1 (casp-1) as a biomarker is tightly linked to its progression.[127] Very recently, Liang and co-workers combined the biocompatible CBT−Cys condensation reaction with the NIR aggregation-induced emission (AIE) dye quinolone malononitrile triphenylamine (QMT) and a casp-1 activation peptide motif (Ac-WEHD) and developed the dual-aggregation-enhanced NIR fluorescent E-MISA probe **3** for highly sensitive in vivo imaging of AD.[128] Probe **3** (QMT-CBT) could be activated to undergo intermolecular cyclization to form QMT-Dimer in the presence of both casp-1 and GSH (triggering the QMT dye's first aggregation). The QMT-Dimers were followed by self-assembly to form QMT-containing NIR AIE fluorescent nanoparticles (QMT-NPs), which achieved the second aggregation and enhancement of NIR FLI (Figure 2g).[128] Following i.v. injection of E-MISA probe **3** into AD mice, the casp-1- and GSH-triggered E-MISA process increased accumulation of "dual AIE" QMT-NPs in the AD region, affording 1.4-fold brighter NIR FLI than its control probe (which relied solely on AIE without self-assembly) (Figure 2h). This enhanced NIR FLI signal could be utilized for the sensitive diagnosis of AD in living mice.

Although E-MISA probes had offered high sensitivity and specificity for molecular imaging of enzymatic activity in living animals via FLI, they were not efficient for the detection of deep-seated enzymes due to the inherent shallow tissue penetration ability of light in biological tissues.

3.2. E-MISA Probes for MRI of Enzymatic Activity

MRI is a clinical imaging tool with high spatial resolution and unlimited tissue penetration depth, allowing the construction of three-dimensional (3D) anatomical images.[129−131] How-
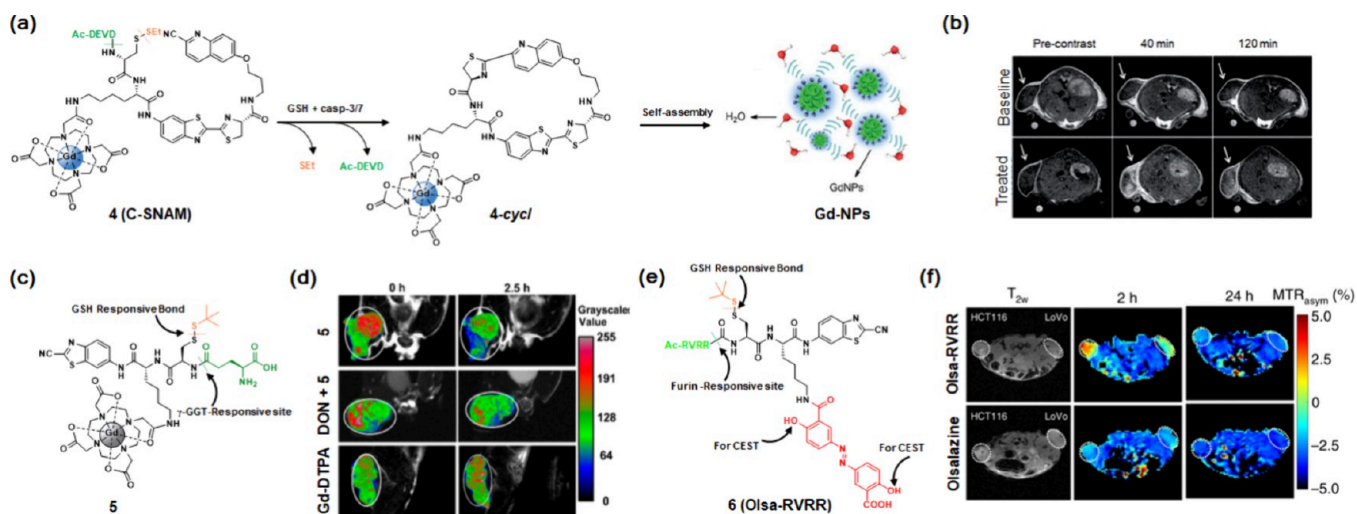
Figure 3. Chemical structures of E-MISA MRI probes. (a) Chemical structure of E-MISA MRI probe **4** and its proposed chemical conversion process in the presence of both GSH and casp-3/7. (b) Representative T_1-weighted images from DOX-treated (Treated) or untreated (Baseline) HeLa tumors following i.v. injection of probe **4** (0.1 mmol/kg). Images were captured at 0 (precontrast), 40, or 120 min. (c) Chemical structure of E-MISA probe **5** for MRI. (d) T_2-weighted coronal MR images of HeLa tumor-bearing mice following (top) i.v. injection of probe **5** (0.08 mmol/kg), (middle) pretreatment with GGT inhibitor 6-diazo-5-oxo-L-norleucine (DON) (0.25 mmol/kg) for 0.5 h and then i.v. injection of probe **5** (0.08 mmol/kg) and (bottom) i.v. injection of Gd-DTPA (0.08 mmol/kg). Images were captured at 0 and 2.5 h. (e) Chemical structure of E-MISA MRI (for CEST) probe **6**. (f) Representative dynamic T_2-weighted (T_{2w}) and Olsa CEST serial MRI images of tumor-bearing mice following i.v. injection of 0.02 mmol/kg probe **6** or free olsalazine (left, HCT116; right, LoVo). Reproduced with permission from ref 97 (copyright 2014 Royal Society of Chemistry), ref 91 (copyright 2019 American Chemical Society), and ref 93 (copyright 2019 the authors of ref 93, under exclusive license to Springer Nature).

ever, MRI has low detection sensitivity for molecular imaging of enzymatic activity, which generally requires the administration of contrast agents to increase the contrast. The development of enzyme-activated contrast agents is highly demanded for in vivo molecular MRI. In 2014, Rao's group reported the first example of a casp-3/7-activatable Gd-based contrast agent (probe **4**, named C-SNAM) using the E-MISA strategy. Probe **4** possessed the same E-MISA scaffold as probe **1**, with a paramagnetic Gd-DOTA chelate in place of the Cy5.5 fluorophore.[97] As with probe **1**, probe **4** could undergo intramolecular cyclization in the presence of casp-3/7 and GSH, leading to the formation of Gd-containing nanoparticles (GdNPs). The GdNPs have a substantially larger molecular size than small-molecule probe **4**, which resulted in the rotation of the Gd chelates being restricted. Consequently, the tumbling time (τ_R) of the Gd chelates was significantly prolonged, accompanied by an enhancement in the r_1 relaxivity (Figure 3a). This E-MISA process increased the r_1 relaxivity from ∼10.2 to ∼19.0 mM^{-1} s^{-1} at 1 T after interaction with casp-3/7 and GSH. This, in conjunction with enhanced accumulation of GdNPs in the apoptotic tumor cells, could produce substantially enhanced T_1-weighted MRI contrast in the s.c. HeLa tumors following chemotherapy or radiotherapy (Figure 3b).[98] It was demonstrated that probe **4** could map the heterogeneous distribution of radiotherapy-induced apoptosis signals within HeLa tumor tissues via high-resolution MRI. The enhanced MRI contrast observed in response to casp-3/7 and GSH in probe **4** was subsequently applied for the in vivo detection of apoptosis in rat adipose-derived stem cells (rASCs).[99]

Gd-based contrast agents could also be utilized for T_2-weighted MRI, depending on the T_1/T_2 ratio at different magnetic fields.[132] In 2019, Liang and colleagues reported the γ-glutamyl transferase (GGT)-activatable Gd-based E-MISA probe **5** for T_2-weighted MRI of GGT activity (Figure 3c).[91]

Upon incubation with GGT and reducing agents, probe **5** could undergo an intermolecular cyclization process. This then self-assembled into spherical GdNPs, resulting in a significant increase in r_2 relaxivity (from 5.20 to 27.8 mM^{-1} s^{-1} at 9.4 T). Probe **5** could produce a dark T_2-weighted MR contrast in the s.c. HeLa tumors at 2.5 h after i.v. injection, which could be inhibited by 6-diazo-5-oxo-L-norleucine (DON) (Figure 3d). In addition to Gd-based contrast agents, the E-MISA strategy based on the biocompatible CBT−Cys reaction has also been successfully applied to build enzyme-activatable superparamagnetic iron nanoparticles (SPIONs) for T_2-weighted MRI.[133−135] Gd-based contrast agents have been widely used for clinical MRI due to their high relaxivity to enhance MR contrast. However, the potential release of free Gd^{3+} ions from the Gd-based contrast agents in vivo might cause side toxicity to patients, particularly for patients with renal dysfunction. More stable organic ligands toward Gd^{3+} would be helpful to reduce the side toxicity relating to the free Gd^{3+}.[136] In addition, it is also highly demanded to develop other paramagnetic-ion-based MR contrast agents (e.g., Mn^{2+}).

Chemical exchange saturation transfer (CEST) is another newly emerging MRI technique that maps the chemical exchange between protons of a probe applied and the protons of bulk water molecules under saturation with irradiation with a suitable radiofrequency.[137] CEST is attractive for molecular MRI of biological processes using a specific CEST probe. In 2019, Bulte and collaborators employed the biocompatible CBT−Cys reaction to build a furin-activatable CEST probe.[93] By linking olsalazine (Olsa), a DNA methylation inhibitor, to the CBT scaffold, they designed probe **6** (named Olsa-RVRR). Probe **6** could undergo an efficient E-MISA process in response to furin and GSH, forming Olsa-containing nanoparticles (Olsa-NPs) with a large number of hydroxyl protons (from Olsa) on the surface. These hydroxyl protons could exchange with bulk protons in the surrounding water
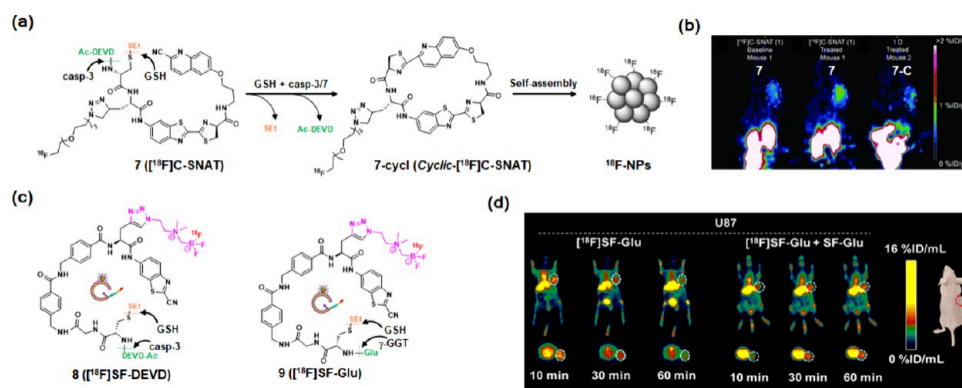
Figure 4. Chemical structures of E-MISA PET probes and their proposed chemical conversion mechanisms. (a) Chemical structure of E-MISA PET probe **7** and its proposed chemical conversion process in the presence of both GSH and casp-3/7. (b) Representative PET images depicting HeLa tumor-bearing mice at 125 min with the indicated treatments. All mice received an i.v. injection of probe **7**, with specific dosages administered to each group: The baseline mouse (left) received probe **7** at 7.8 MBq/211 mCi. The DOX-treated mouse (middle) received probe **7** at 12 MBq/324 mCi. Another DOX-treated mouse (right) received the control probe **7-C** (which cannot be cleaved by casp-3/7) at 5.4 MBq/146 mCi. The tumor region is indicated by the white dashed circle on the right shoulder of each mouse. (c) Chemical structures of E-MISA PET tracer probes **8** and **9**. (d) Transversal and coronal PET images of U87 tumor-bearing mice after i.v. injection of probe **9** (∼3.7 MBq) from 10 to 60 min. Reproduced with permission from refs 100 and 92. Copyright 2013 Wiley-VCH and 2022 American Chemical Society, respectively.

molecules, resulting in distinct CEST signals (Figure 3e). Enhanced accumulation of Olsa-NPs in the probe **6**-treated furin-positive HCT116 tumors was achieved, resulting in a significantly higher CEST contrast compared to that of free Olsa-treated mice or furin-deficient LoVo tumors (Figure 3f).

3.3. E-MISA Probes for PET of Enzymatic Activity

PET imaging, based on the detection of high-energy γ photons emitted from radionuclides, has been widely used in clinical settings due to its high detection sensitivity and tissue penetration depth.[138−140] Strategies that allow for selective accumulation of radionuclides in target tissues are crucial for PET imaging. Generally, radiolabeling of enzyme inhibitors or antibodies is a commonly used strategy to build PET tracers toward enzymes or receptors. These PET tracers could produce enhanced imaging signals through binding to the target enzymes or receptors, with the enhancement signals largely dependent on the number of target enzymes or receptors. Alternately, the E-MISA strategy could leverage the catalytic activity of the target enzyme to promote the retention of the radionuclides in targeted tissues, which could offer a smart approach to build PET tracers for in vivo imaging. In 2013, Rao and colleagues employed the biocompatible CBT−Cys condensation reaction and developed the ^{18}F-labeled E-MISA PET probe **7** (named [^{18}F]C-SNAT) for PET imaging of casp-3/7 activity in vivo.[100,101] Probe **7** could be cleaved by casp-3/7 and reduced by GSH, followed by intramolecular cyclization and self-assembly into ^{18}F-labeled nanoparticles (^{18}F-NPs) (Figure 4a). The in situ-formed ^{18}F-NPs demonstrated the ability to retard washout and prolong retention in apoptotic tumor cells, thereby allowing for the trapping of a greater quantity of ^{18}F radionucleotides in apoptotic tumor cells relative to viable tumor cells. PET imaging in vivo showed that probe **7** could produce higher PET signals in the HeLa tumors after treatment with DOX compared to prior treatment (Figure 4b). It was found that probe **7** could outcompete other PET tracers (e.g., ^{18}F-FDG, ^{99m}Tc-Annexin V and ^{18}F-ML-10) for in vivo imaging of drug-induced apoptosis in tumor tissues. These results demonstrated that the E-MISA strategy has the potential to be a valuable tool for PET imaging of tumor apoptosis.[102]

Based on probe **7**, Lin and co-workers recently optimized the E-MISA scaffold by introducing two *p*-aminobenzoic acid moieties and using CBT instead of the CHQ group. The new scaffold showed improved reaction kinetics and stability for radiolabeling. They developed the ^{18}F-labeled E-MISA PET probe **8** (labeled as [^{18}F]SF-DEVD) for PET imaging of casp-3 (Figure 4c).[92] Findings showed that probe **8** could similarly produce strong PET signals in the drug-treated HeLa tumor via coinjection with its cold compound. Using the optimized E-MISA scaffold, they further developed a GGT-activated PET tracer (probe **9**, also named [^{18}F]SF-Glu) for sensitive imaging of GGT-overexpressing U87MG tumors (Figure 4d). The E-MISA-enabled approach could also be applied for the development of a smart ^{68}Ga-labeled PET tracer for in vivo imaging of furin activity.[94]

3.4. E-MISA Probes for PAI of Enzymatic Activity

PAI is an emerging imaging modality that utilizes pulsed laser irradiation and acoustic detection and is a powerful tool for the detection of tumors and other diseases. PAI has the advantages of high sensitivity, high spatial resolution, and high imaging depth for in vivo imaging.[141−143] To achieve activatable PAI probes, Gambhir and colleagues first employed the enzyme-activatable strategy to develop the first furin-responsive PAI probe (**10**, ESOR-PA01) for in vivo imaging of furin activity. This probe was designed by introducing an NIR fluorescent dye, Atto-740, to the scaffold of the CBT−Cys system to provide PAI signals (Figure 5a).[95] In the presence of both furin and GSH in tumor cells, probe **10** could be triggered to proceed with intermolecular condensation to form dimers and oligomers. Then the dimers and oligomers could be self-assembled into Atto-740-containing nanoparticles, which led to efficient quenching of the NIR fluorescence of Atto-740 in the nanoparticles resulting from the aggregation-caused quenching (ACQ) effect. The nonradiative relaxation process was enhanced, and more energy could be converted into heat, thereby producing the higher PA intensity. After injection into mice, probe **10** could produce a significant ∼7.1-fold higher PA intensity in furin-overexpressing MDA-MB-231 tumors than in furin-deficient LoVo tumors (Figure 5b).
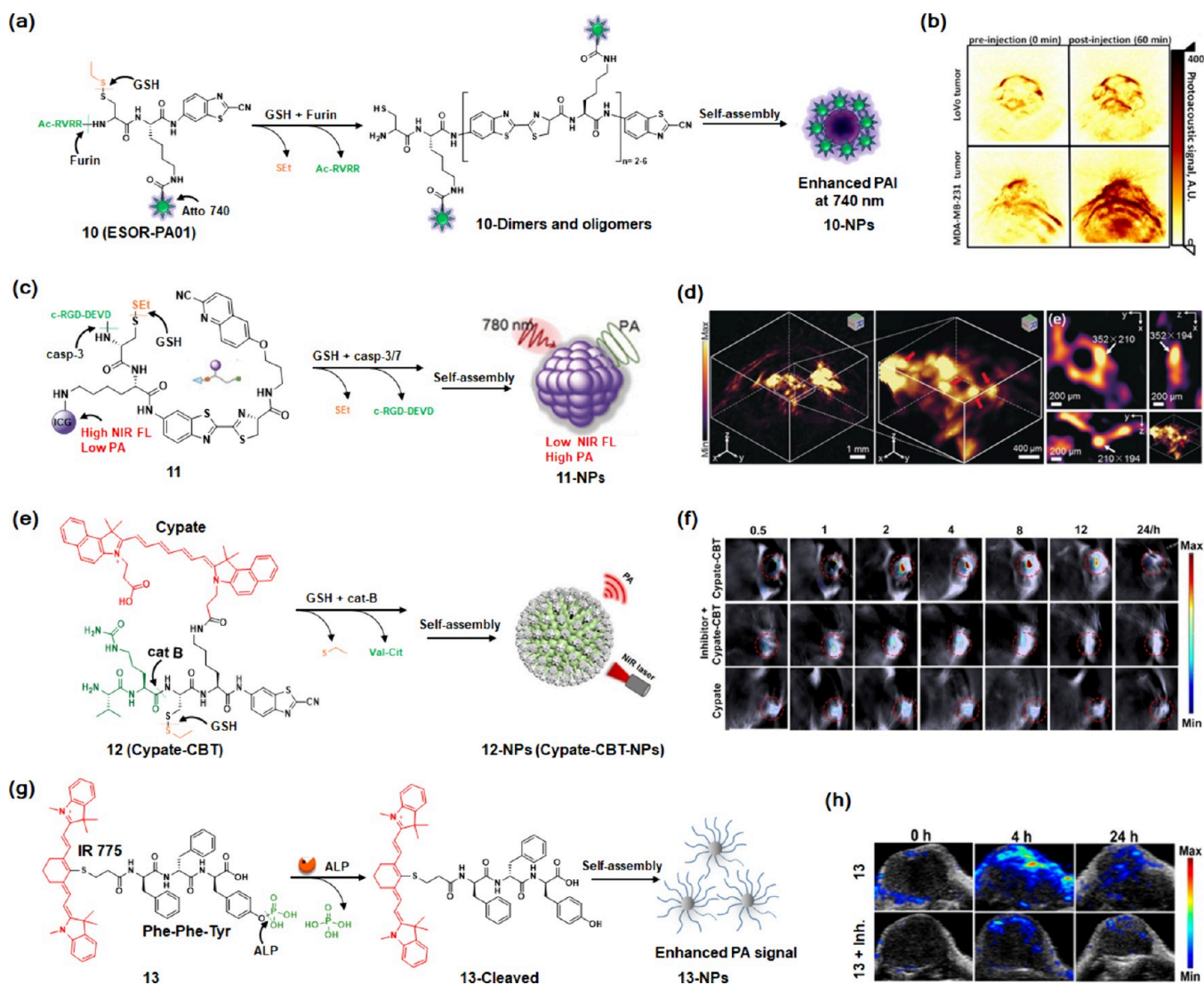
Figure 5. Chemical structures of E-MISA PA probes and their proposed chemical conversion mechanisms. (a) Chemical structure of furin-activatable PA probe **10** and its mechanism for the generation of PA contrast in the presence of both GSH and furin. (b) Representative PA images displaying (top) a furin-deficient LoVo tumor and (bottom) a furin-overexpressing MDA-MB-231 tumor in mice. Images were captured at two time points: before (0 min) and after i.v. injection (60 min) of furin-activatable PA probe **10**. (c) Chemical structure of E-MISA PET probe **11** and its proposed chemical conversion process in the presence of both GSH and casp-3/7. (d) Representative 3D reconstruction PA image and its corresponding enlarged area for the apoptotic region of a DOX-treated HeLa tumor after i.v. injection of probe **11** (20 nmol) at 10 h. (e) Chemical structure of E-MISA PA probe **12** and its proposed chemical conversion process in the presence of both GSH and cat-B. (f) Representative PA images of cat B-overexpressing MDA-MB-231 tumor-bearing mice following (top) intratumoral (i.t.) injection of probe **11**, (middle) pretreatment with the cat B inhibitor CA-074-Me for 30 min followed by i.t. injection with probe **11**, and (bottom) i.t. injection of free cypate. Images were captured from 0.5 to 24 h following i.t. injection of probe **12**. (g) Chemical structure of E-MISA PA probe **13** and its proposed chemical conversion process in the presence of ALP. (h) Representative PA images of (top) untreated HeLa tumor-bearing mice following i.t. injection of probe **13** or (bottom) HeLa tumor-bearing mice pretreated with the ALP inhibitor L-phenylalanine and then i.t. injected with probe **13** after 30 min. Images were presented before (0 h) and after injection (4 and 24 h) of probe **13**. Reproduced with permission from refs 95, 103, 109, and 79. Copyright 2013 American Chemical Society, 2019 Wiley-VCH, 2021 Wiley-VCH, and 2018 American Chemical Society, respectively.

In 2019, Ye and colleagues developed the first casp-3/7-activatable E-MISA PA probe, designated as probe **11**, for PAI detection of casp-3/7 activity in vivo (Figure 5c).[103] To improve the active targeting capability of probe **11**, they incorporated a cyclic RGD ligand (c-RGD) into the N-terminal region of the DEVD peptide. Upon cleavage by casp-3/7 and reduction by GSH, both the c-RGD-DEVD peptide and the disulfide bond were removed, initiating subsequent intramolecular cyclization and the in situ self-assembly process to form indocyanine green (ICG)-containing nanoparticles (**11**-NPs). The NIR FL of **11**-NPs at 810 nm was quenched by

approximately 22-fold due to the ACQ effect of the aggregated ICG in the **11**-NPs. However, the PA signal at 780 nm was significantly enhanced (approximately 3-fold increased), resulting in a high PAI signal. Following i.v. injection of probe **11** into DOX-treated U87MG tumor-bearing mice, the hydrophilic probe could be actively delivered into the tumor tissue via the c-RGD ligand, which specifically targets the overexpressed $\alpha_v\beta_3$ integrin receptor on the tumor surface, facilitating its internalization by tumor cells. Upon entering apoptotic tumor cells, which were positive for casp-3/7 and GSH, probe **11** underwent a transformation into PA-enhanced
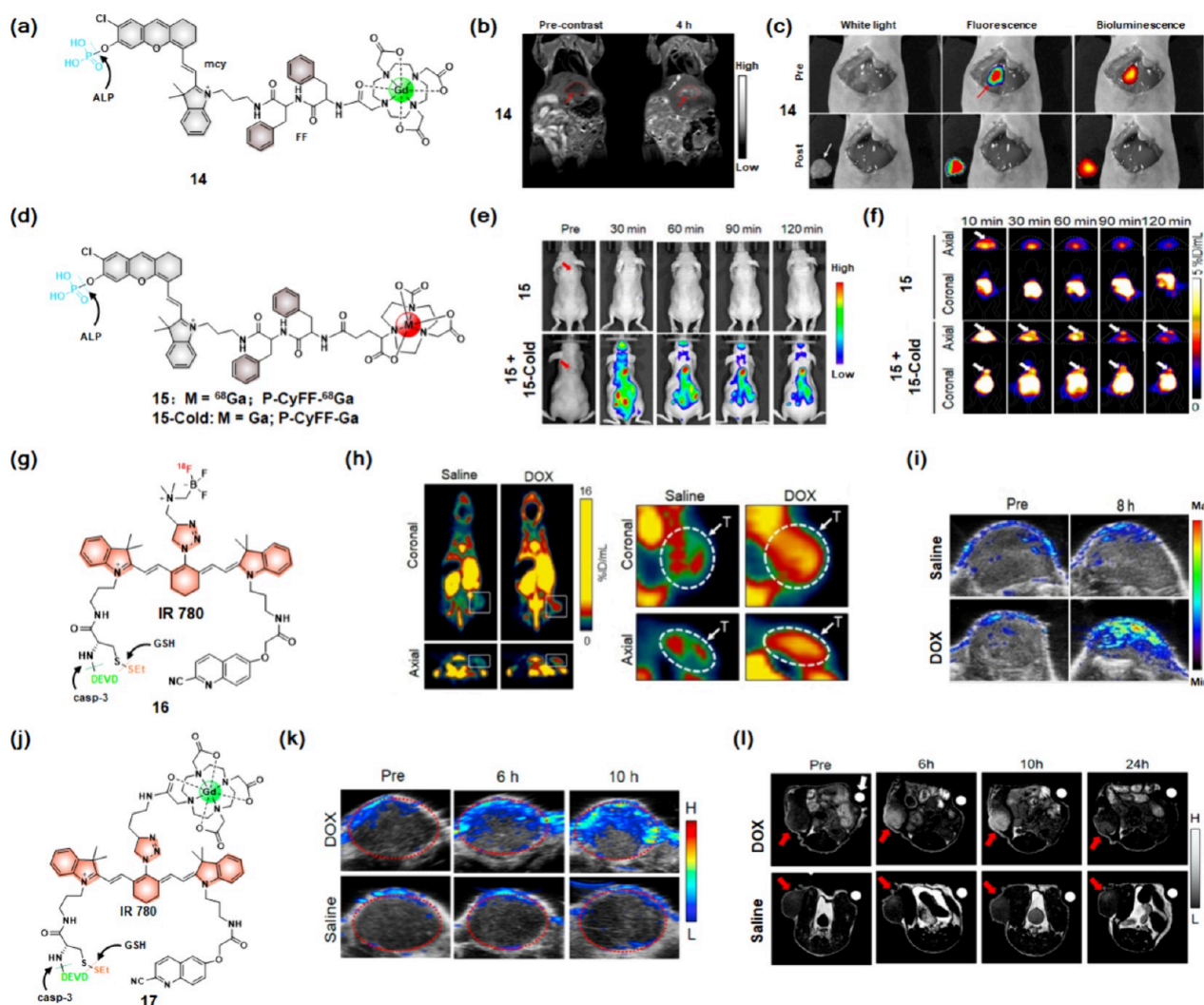
Figure 6. E-MISA multimodality imaging probes and their chemical structures. (a) Chemical structure of NIR FLI/MRI bimodal probe **14**. (b) Representative MRI images of orthotopic HepG2/Luc liver tumor xenograft mice before (Precontrast) and 4 h after injection of probe **14** (0.015 mmol kg^{-1}), (c) NIR FLI-guided surgical resection of orthotopic HepG2/Luc liver tumor in an intraoperative mouse by directly spraying probe **14** (10 μM) on the liver. (d) Chemical structures of NIR FLI/PET bimodal probe **15** and its cold probe **15-Cold**. (e) Longitudinal NIR FLI and (f) PET imaging of HeLa tumor-bearing mice with the indicated treatments. The images were acquired at 0, 30, 60, 90, and 120 min after i.v. injection of probe **15** (~7.4 MBq) or coinjection with probes **15** (~7.4 MBq) and **15-Cold** (50 μM, 200 μL). Arrows indicate the tumor sites. (g) Chemical structure of E-MISA probe **16**, which was utilized for the PAI/PET bimodality imaging of casp-3 activity in vivo. (h) Representative axial and coronal PET images of U87MG tumors in living mice at 1 h after i.v. coinjection of probe **16** (~7.4 MBq) and its cold probe (40 nmol). White boxes indicate the tumor sites. Enlarged PET images of the tumor sites are shown at the right. T indicates the tumor site in each image. (i) Representative PAI images (overlaid with ultrasound mode) of DOX-treated (DOX) or saline-treated (Saline) U87MG tumor-bearing xenograft mice before (Pre) and 8 h after i.v. injection of probe **16** (40 nmol). (j) Chemical structure of E-MISA probe **17**, which was used for PAI/MRI bimodality imaging of casp-3 activity in vivo. (k, l) Representative (k) PA images (overlaid with ultrasound images, at 855 nm) and (l) T_1-weighted MR images of DOX-treated (DOX) or saline-treated (Saline) U87MG tumor-bearing xenograft mice at baseline (Pre) or various time points after i.v. injection of probe **17** (0.1 mmol/kg). Reproduced with permission from refs 80, 81, 104, and 105. Copyright 2019 American Chemical Society, 2021 American Chemical Society, 2022 Wiley-VCH, and 2022 Elsevier B.V., respectively.

11-NPs and was trapped within tumor cells. In addition, the authors found that high-resolution reconstructed 3D PA images display the **11**-NPs, which were subsequently trapped within the tumor tissues, allowing for precise evaluation of the DOX chemotherapy response of tumors in the early stages (Figure 5d).

In addition to the assessment of casp-3/7 activity using the E-MISA PA probe, in 2021 Liang and colleagues introduced the cat B-activatable E-MISA PA probe **12** (Cypate-CBT) for PAI of cat B activity in vivo (Figure 5e).[109] Different from probe **11**, they incorporated a cat B-responsive dipeptide motif (Val-Cit) at the N-terminus of the D-Cys residue and an NIR

fluorophore, cypate, for PAI. Upon cleavage by cat B and reduction by GSH, both the Val-Cit dipeptide and the disulfide bond were removed, initiating subsequent intermolecular cyclization and in situ self-assembly to form cypate-containing PA-enhancement nanoparticles (**12**-NPs). Following intra-tumoral (i.t.) injection of probe **12** into cat B-overexpressing MDA-MB-231 tumor-bearing mice, fast cleavage by cat B and reduction by GSH led to intermolecular cyclization and self-assembly, resulting in significant PAI enhancement. In vivo PAI data show that probe **12** exhibited significantly enhanced PAI in MDA-MB-231 tumors compared to free cypate-treated

mice or mice pretreated with cat B inhibitor (CA-074-Me) and then treated with probe **12** (Figure 5f).

Different from the biocompatible CBT–Cys condensation reaction-triggered self-assembly process, the enzyme-triggered proteolysis E-MISA strategy involves the direct manipulation of enzyme-cleaved products to undergo in situ self-assembly into nanoaggregates in vivo. ALP, a key clinical diagnostic biomarker, is extensively present in biological tissues and associated with various diseases such as liver disease, bone disease, and some malignant tumors.[144] In 2018, Liang and collaborators reported the first ALP-sensitive E-MISA PA probe **13** for in vivo PAI of ALP activity. Probe **13** comprised an ALP-recognition hydrophobic Phe-Phe-Tyr(H_2PO_3) tripeptide and the NIR dye IR775 for PAI.[79] The hydrophilic H_2PO_3 group on the Tyr ensures that probe **13** maintains a high water solubility and is a small molecule in solution, resulting in a low PA signal. However, upon dephosphorylation by ALP, the H_2PO_3 group was removed, resulting in rapid conversion of probe **13** into a more hydrophobic enzyme-cleaved product (**13**-cleaved). The intermolecular hydrophobic force of **13**-cleaved was significantly enhanced as a result of the chemical structure being converted, which promoted the in situ self-assembly process and the transformation of the molecule into IR775-containing PA-enhancement nanoparticles (**13**-NPs) (Figure 5g). Following the i.t. injection of probe **13** into ALP-overexpressing HeLa tumor-bearing mice, a consistently enhanced PAI signal was produced via the ALP-mediated self-assembly process, resulting in a 2.3-fold increase in PA intensity compared to that observed in HeLa tumors pretreated with the ALP inhibitor L-phenylalanine at 4 h (Figure 5h)

3.5. E-MISA Probes for Multimodality Imaging of Enzymatic Activity

The integration of two or more complementary imaging modalities, known as multimodality imaging, provides a comprehensive image of the regions of interest. These approaches have been widely employed for molecular imaging and/or imaging-guided theranostics.[145−147] In recent years, several E-MISA multimodality imaging probes have been developed for reliable imaging of enzyme activity for diagnosis of tumors or imaging-guided tumor resection in vivo.[148,149]

MRI can produce anatomical images with unlimited tissue penetration depth and high spatial resolution to promote preoperative detection of deep-seated tumors; NIR FLI is a highly sensitive imaging technique that could be employed for the detection of low concentrations of tumor-associated biomarkers.[150] Thus, integration of the advantages of NIR FLI and MRI could be conducted with high-sensitivity and high-spatial-resolution imaging of enzymes in vivo. In 2019, Ye and co-workers employed the E-MISA strategy to design the ALP-activatable NIR FLI/MRI bimodality probe **14** (P-CyFFGd) for in vivo imaging of ALP activity.[80] Probe **14** contained the H_2PO_3-group-caged NIR dye merocyanine (mcy) for activatable NIR FLI, the Gd-based chelate DOTA-Gd for activatable MRI, and a hydrophobic dipeptide D-Phe-D-Phe (FF) linker to promote self-assembly (Figure 6a). Probe **14**, which exhibited an "OFF" NIR FLI and low r_1 relaxivity, was a water-soluble small-molecule probe that was dispersed uniformly in solution due to the presence of the hydrophilic H_2PO_3 group and a DOTA-Gd chelate. Upon dephosphorylation by ALP, the H_2PO_3 group of probe **14** was removed, resulting in the formation of an amphiphilic cleaved product

(CyFF-Gd). Subsequently, CyFF-Gd underwent the in situ self-assembly process to form the NIR FLI signal (>70-fold enhancement) and MRI signal (∼2.3-fold r_1 relaxivity enhancement) concurrently enhanced nanoparticles (**14**-NPs). Following i.v. injection of probe **14** into ALP-positive HeLa tumor-bearing mice, stronger NIR FLI/MRI bimodal imaging signals were presented at tumor sites compared to that of nonassembling control probe-treated mice (P-Cy-Gd). Additionally, probe **14** was used for the preoperative detection of orthotopic liver HepG2 tumors via high-spatial-resolution T_1-weighted MRI, followed by imaging-guided resection of the tumor intraoperatively using sensitive NIR FLI (Figures 6b,c).

PET imaging offers high tissue penetration depth, while FLI provides a high-sensitivity imaging signal. The combination of these two techniques may result in the simultaneous achievement of high tissue penetration depth and high-sensitivity imaging in vivo.[151,152] Moreover, coinjection of radioisotope-free cold E-MISA probe with its radioisotope-hot counterpart could further reduce the dosage of the radio-isotope-hot probe required in vivo. Based on the idea and the foundation of probe **14**, Ye and colleagues reported the NIR FLI/PET bimodal E-MISA probe **15** (P-CyFF-^{68}Ga), replacing the former Gd-DOTA chelate of probe **14** with the radioisotope NODA-^{68}Ga for NIR FL/PET bimodality imaging of ALP in vivo (Figure 6d).[81] The hydrophilic H_2PO_3 group and NODA-Ga chelate render probe **15** (^{68}Ga) or probe **15**-Cold (^{69}Ga) as water-soluble small-molecule probes that were uniformly dispersed in solution. This results in the quenching of NIR FLI. Following i.v. injection of probe **15** or coinjection of probes **15** and **15**-Cold into HeLa tumor-bearing mice, bright NIR FLI was observed in the tumor region of the coinjection-treated group, which was ∼6.2-fold higher than that in the probe **15**-treated group at 30 min (Figure 6e). The E-MISA process resulted in the in situ formation of **15**-NPs, which were reduced in diffusion and prolonged in retention. This was demonstrated by a markedly elevated NIR FL in the coinjection of probe **15**- and **15**-Cold-treated mice in comparison to that of mice treated only with probe **15**, which was consistent with the PET imaging results (Figure 6f).

PAI can offer relatively high sensitivity, spatial resolution, and deep tissue penetration, but it is unable to perform whole-body imaging. Integrating it with whole-body-sensitive imaging techniques like PET indeed offers a promising approach for fast locating the disease foci in the whole body via PET imaging. After that, PAI can be employed to further conduct high spatial-resolution 3D imaging at interest regions.[153] In 2022, Ye and colleagues reported the PET/PAI bimodality E-MISA probe **16** ([^{18}F]-IR780-1) by employing a new triazole-IR 780 fluorescent scaffold and the CBT–Cys condensation reaction for in vivo imaging of casp-3 activity in tumor apoptosis cells (Figure 6g).[104] Upon i.v. injection of probe **16** into DOX-treated U87MG tumor-bearing mice, it underwent an intramolecular condensation reaction and was transformed into PAI/PET bimodal signal enhancement **16**-NPs, which were trapped within apoptosis tumor cells at the casp-3/7- and GSH-positive regions. This process resulted in significantly enhanced PAI/PET bimodal signals at the apoptosis tumor region. In vivo imaging data demonstrated that leveraging PET for high sensitivity whole-body imaging signals enables quick localization of tumor foci, followed by high-spatial-resolution PA imaging (at 855 nm) for detailed visualization of the tumor regions (Figure 6h,i). This strategy has the potential to serve as
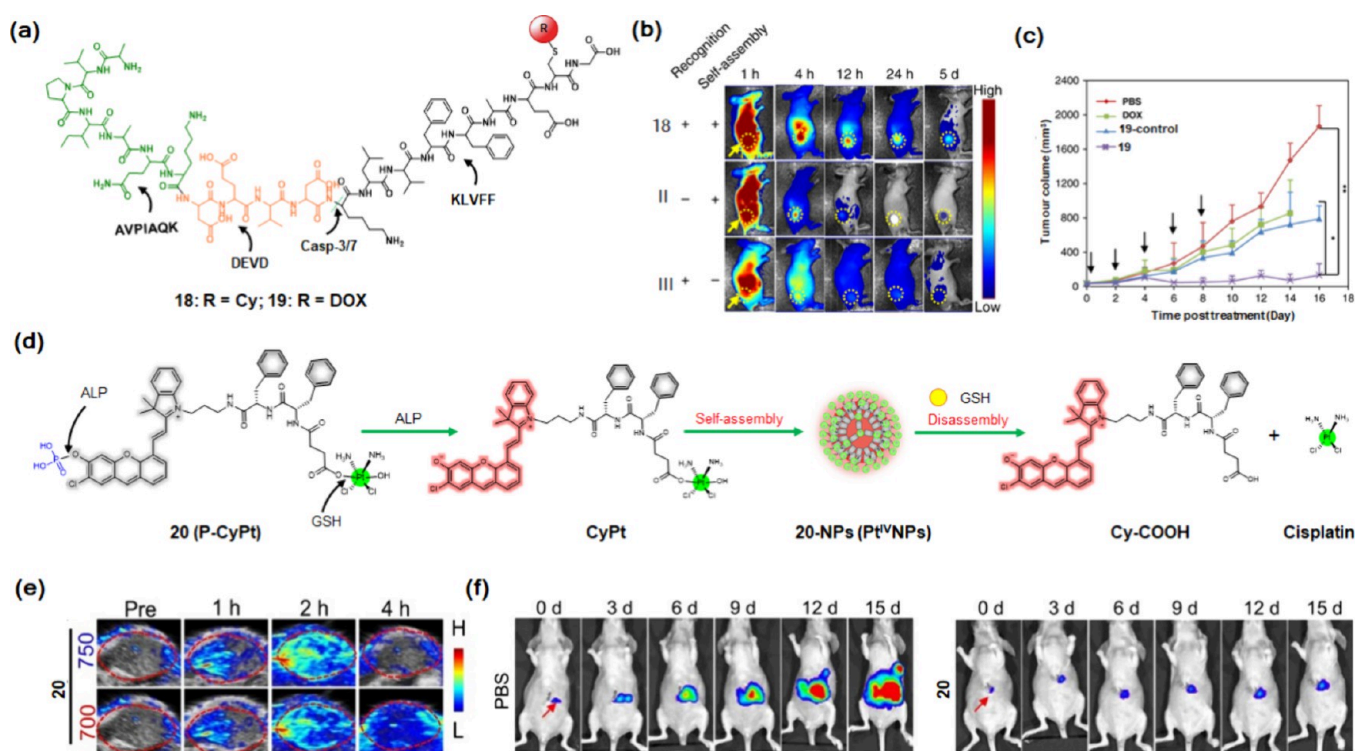
Figure 7. Chemical structures of E-MISA theranostic with chemotherapy probes 18, 19, and 20 (containing chemodrugs). (a) Chemical structures of probes **18** and **19**. (b) Longitudinal NIR FLI of H460 tumor-bearing mice after i.v. injection of probe **18** and its control probes (II lacking the recognition unit and III lacking the self-assembly unit compared with probe **18**). The images were obtained at 1, 4, 12, and 24 h and 5 days postinjection. (c) Tumor volume changes of H460 tumor-bearing mice after i.v. injection of PBS, free DOX, **19-control**, or **19** (based on the DOX dosage of 2.0 mg/kg). Black arrows indicate the i.v. injection time. (d) Chemical structure of probe **20** and its proposed sequential ALP-triggered dephosphorylation self-assembly and following GSH-triggered disassembly process mechanism. (e) Representative dual channels of PA images (at 700 and 750 nm) of HeLa tumor-bearing mice that received an i.v. injection of probe **20** (100 μM, 200 μL) at 0 (pre), 1, 2, 4, and 8 h. (f) Representative bioluminescence (BL) images of HepG2/Luc orthotopic liver tumor-bearing mice at 0, 3, 6, 9, 12, and 15 days following PBS or probe **20** (2.25 mg kg^{-1} Pt, 200 μL i.v. injection at days 0, 3, 6, 9, and 12) treatments. The red arrows indicate the tumor site nodules in the liver region. Reproduced from refs 106 (CC BY 4.0) and 82 (CC BY 4.0).

a powerful tool for assessing early chemotherapy response efficacy and tailoring therapeutic regimens for patients, as it allows for the precise localization and characterization of the tumor sites.

In addition to precise PAI/PET bimodality imaging of casp-3, a combination of PAI and MRI techniques could provide complementary advantages that overcome the limitations of each technique individually. For instance, PAI has limited tissue penetration, while MRI has low sensitivity.[154] Based on this idea, Ye and colleagues developed the casp-3-activatable E-MISA PAI/MRI bimodal probe **17** (Gd-IR780) in 2022 by replacing the former [^{18}F] trace of probe **16** with the hydrophilic DOTA-Gd chelate, for in vivo imaging of apoptosis tumor cells (Figure 6j).[105] Following i.v. injection of probe **17** into saline- or DOX-treated U87MG tumor-bearing mice, a significant enhancement in PAI (~20.4-fold) and MRI (~4.28-fold) signals was observed in the DOX-treated tumors compared to the saline-treated tumors at 10 h post-injection (Figures 6k,l). This strategy holds the potential to enhance the capabilities of molecular imaging, providing improved sensitivity and spatial resolution, which will facilitate more accurate characterization of tumor apoptosis.

4. E-MISA PROBES FOR THERANOSTICS

Theranostic probes, which combine imaging and therapy to allow imaging-guided therapy, are a promising tool for precision medicine. Considering that the E-MISA strategy could enhance the accumulation of various imaging moieties at the target tissues for in vivo imaging of different enzyme activities, the integration of therapeutic functions into the E-MISA strategy could be amenable to the design of enzyme-activatable therapeutic probes for imaging-guided on-demand therapy.[155−157] Currently, a number of E-MISA theranostic probes have been reported by integrating different imaging modalities with different therapeutic modes, such as chemotherapy, phototherapy (e.g., photodynamic therapy (PDT) and photothermal therapy (PTT)), SDT and combination therapy.

4.1. E-MISA Theranostic Probes for Chemotherapy

Chemotherapy has been extensively utilized for cancer therapy in clinics, providing essential means to improve survival rates and quality of life for patients with various types of cancer.[158] The chemotherapeutic efficacy against malignant tumors in vivo is highly dependent on the efficient delivery and accumulation of chemodrugs in tumor tissues.[159] To enable enhanced delivery and retention of DOX in tumors, Wang and colleagues proposed a tumor-selective cascade-activatable self-detained system (TCASS) and designed two casp-3-responsive E-MISA theranostic probes (**18** and **19**) for NIR FLI and chemotherapy of tumors.[106] These probes consisted of a peptide sequence (AVPIAQK) capable of targeting the X-linked inhibitor of apoptosis protein (XIAP), a DEVD substrate peptide specifically recognized by casp-3/7, a
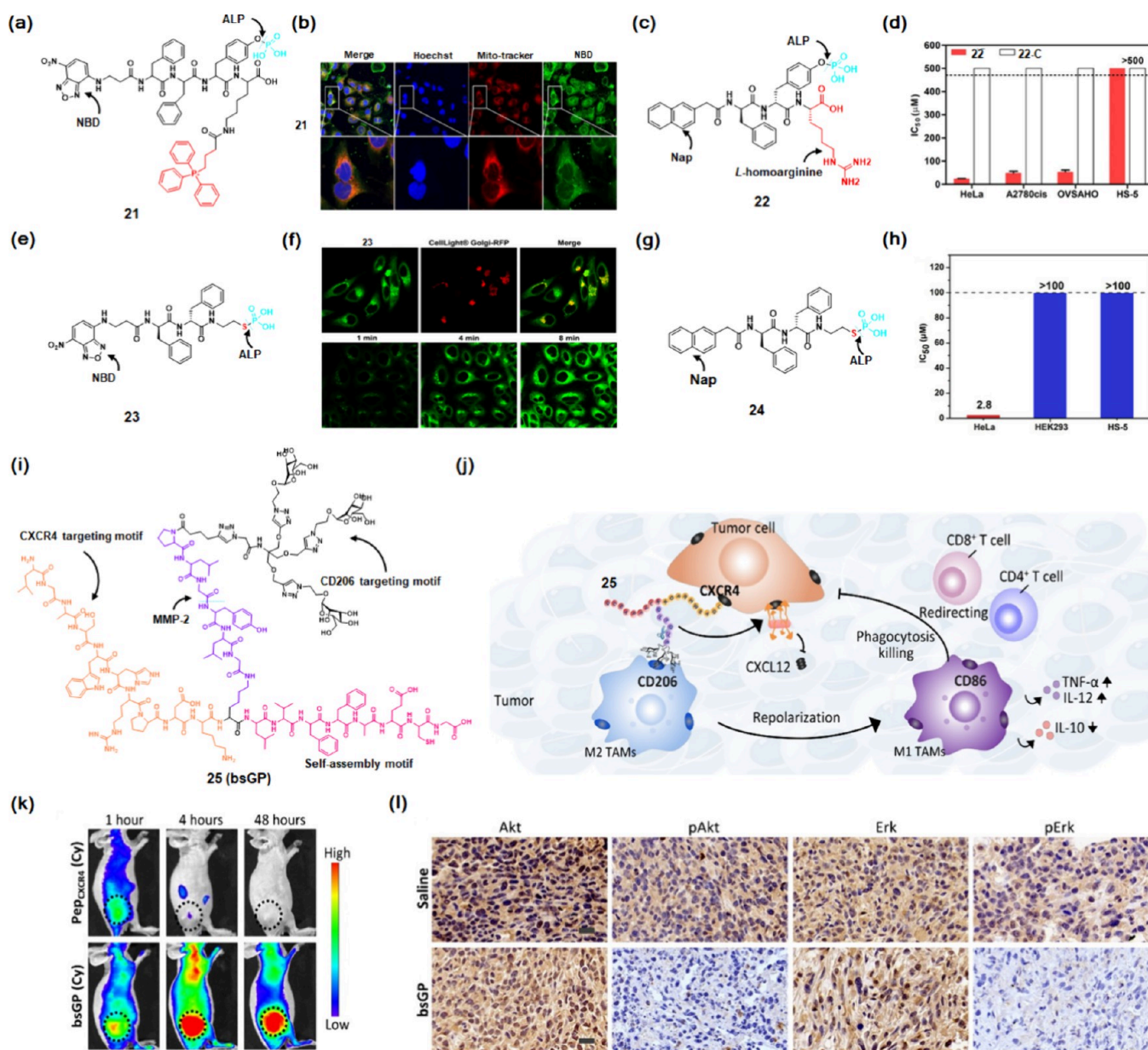
Figure 8. Chemical structures of E-MISA theranostic probes (not containing chemodrugs) for chemotherapy. (a) Chemical structure of probe **21**. (b) Confocal imaging of Saos2 cells after incubation with probe **21** (containing D-amino acid residues) for 4 h followed by staining with Mito-tracker. (c) Chemical structure of probe **22**. (d) IC_{50} values (24 h) of probe **22** and its control probe **22-C** (lacking the H_2PO_3 group) against ALP-positive HeLa, A2780cis, and OVSAHO cancer cells and ALP-negative normal HS-5 cells. (e) Chemical structure of probe **23**. (f) Confocal imaging of HeLa cells: in the top row, cells were stained with CellLight Golgi-RFP after being incubated with probe **23** for 8 min; in the bottom row, cells were incubated with probe **23** for 1, 4, and 8 min. (g) Chemical structure of probe **24**. (h) IC_{50} values of probe **24** against ALP-positive HeLa cancer cells and ALP-negative normal HEK-293 or HS-5 cells. (i) Chemical structure of probe **24** and (j) the proposed mechanism to regulate the tumor microenvironment (TME) for inhibiting bladder cancer recurrence. (k) Representative NIR FL images of EJ xenograft mice after i.v. injection of probe **25-Cy** (500 μM, 100 μL) and its control probe Pep_{CXCR4} (500 μM, 100 μL) at 1, 4, and 48 h. The black dotted circles indicate the tumor regions. (l) Representative immunofluorescence staining images of the levels of Akt and Erk and their phosphorylated form products pAkt and pErk in tumor tissues of saline- or probe **25**-treated EJ tumor-bearing mice. Reproduced with permission from refs 83 (copyright 2016 American Chemical Society), (copyright 2018 American Chemical Society), 85 (copyright 2021 Wiley-VCH), and 78 (CC BY-NC 4.0).

hydrophobic peptide (KLVFFAECG) to promote molecular self-assembly into nanofibers (NFs), and a function molecule, cyanine dye (Cy) for NIR FLI (**18**) or DOX for chemotherapy (**19**) (Figure 7a). After i.v. injection of these probes into H460 tumor-bearing mice, the AVPIAQK specifically bonded to tumor cells overexpressing XIAP, triggering the downstream casp-3/7 activation. This activation led to the subsequent cleavage and self-assembly process, resulting in the in situ

transformation of Cy-containing nanofibers (**18**-NFs) or DOX-containing nanofibers (**19**-NFs), which promoted long-term retention and accumulation of NFs within the tumor cells. Consequently, strong NIR FLI and significant anticancer efficacy could be achieved in living mice treated with probe **18** or **19** in vivo (Figures 7b,c).

To visualize the sequential cisplatin prodrug delivery and release process in tumors via the NIR FLI/PAI bimodal

imaging, Ye and colleagues recently developed the E-MISA theranostic probe **20** (P-CyPt) employing an ALP-triggered in situ self-assembly and intracellular GSH-induced disassembly strategy (Figure 7d).[82] Unlike their previously reported E-MISA molecular imaging probes, probe **20** contained a hydrophilic clinical first-line chemodrug, cisplatin prodrug (Pt(IV)), instead of DOTA-Gd (**14**) or NODA-^{68}Ga (**15**), ensuring good water solubility. Upon hydrolysis by ALP, probe **20** self-assembled into dual channels of PA signals (700 and 750 nm) and NIR FLI signals-enhanced Pt(IV) nanoparticles (Pt^{IV}NPs) on the tumor cell membrane. Once these Pt^{IV}NPs were taken up by tumor cells, they could be rapidly reduced by GSH, leading to the burst release of high-cytotoxicity Pt(II) and induction of the disassembly process. Consequently, during the disassembly process, the NIR FLI signal was enhanced again, while the PA signal at 750 nm decreased and the PA signal at 700 nm remained nearly unchanged. This dynamic change in PAI/NIR FLI signals enabled the real-time monitoring of cisplatin prodrug delivery and release. Following i.v. injection of probe **20** into s.c. HeLa tumor-bearing mice, strongly enhanced NIR FLI and significant dual PAI signals were observed at 2 h due to the ALP-triggered in situ self-assembly process. Subsequently, with the succeeding intracellular GSH-induced disassembly initialized, the NIR FLI and PA signals at 700 nm remained strong but the PA signal at 750 nm decreased to the baseline at 4 h (Figure 7e). Moreover, the sequential ALP-triggered in situ self-assembly and intracellular GSH-induced disassembly strategy that enhanced drug delivery and accelerated cisplatin release process effectively suppressed the growth and metastasis of orthotopic HepG2 liver cancer tumors (Figure 7f). In addition to the direct use of cytotoxic chemodrugs, E-MISA theranostic probes capable of selectively accumulating in cellular organelles (e.g., mitochondria, endoplasmic reticulum, and Golgi apparatus) to exert cytotoxicity against tumor cells have also been successfully reported.[160] In 2016, Xu and colleagues developed the first ALP-responsive mitochondria-targeting E-MISA probe (**21**) for selectively killing tumor cells and avoiding the acquired drug resistance (Figure 8a).[83] Probe **21** contained an ALP-recognition hydrophobic Phe-Phe-Tyr(H$_2$PO$_3$)-Lys tetrapeptide, an environment-sensitive fluorophore (4-nitro-2,1,3-benzoxadiazole, NBD) for FLI, and a mitochondria-targeting part (triphenylphosphinium, TPP). Once probe **21** was incubated with ALP-overexpressing cancer tumor (e.g., Saos2) cells, probe **21** was dephosphorylated by ALP and in situ self-assembled into NBD-containing nanoaggregates on the tumor cell membrane. These nanoaggregates were subsequently internalized into lysosomes via an endocytosis process by tumor cells. The authors found that the NBD-containing nanoaggregates could escape from the endosome/lysosome and actively target mitochondria at 4 h (Figure 8b). The large number of TPP groups on nanoaggregates could multivalently combine with the mitochondria, resulting in disruption of the mitochondria function to selectively kill cancer cells. Moreover, the authors demonstrated that this process uses nonspecific cytotoxic agents to selectively kill cancer cells without inducing the acquired drug resistance.

In addition to targeting mitochondria for inducing cancer cell death, specific targeting of the endoplasmic reticulum (ER) can also effectively kill tumor cells. In 2018, Xu's group reported an ER-targeting E-MISA probe for selective killing of cancer cells (Figure 8c).[84] Based on probe **21**, they optimized the E-MISA scaffold by substituting the former NBD group

with a 2-naphthylacetyl (Nap) group to enhance aromatic—aromatic interactions and replaced the former D-lysine residue with a positively charged L-homoarginine residue to facilitate membrane interaction, resulting in the development of E-MISA probe **22**. Once dephosphorylated by ALP, probe **22** underwent in situ self-assembly into Nap-containing crescent-shaped aggregates on the tumor cell membranes. Then the membranes could be disrupted by these aggregates, which were further internalized by tumor cells and subsequently targeted to the ER. Accumulation of a large number of crescent-shaped aggregates could induce ER stress, activating the cascade caspase signals that ultimately led to significant tumor cell death (Figure 8d).

Based on their former probes **21** and **22**, Xu and colleagues lately showed that by replacing the oxygen atom of the H$_2$PO$_3$ group with a sulfur atom, the ALP-responsive Golgi apparatus (GA)-targeting E-MISA probe **23** could be designed to selectively kill tumor cells (Figure 8e).[85] Probe **23** could be rapidly dephosphorylated by ALP and transformed to NBD-containing thiopeptide assemblies after incubation with HeLa cells. These thiopeptide assemblies were rapidly internalized by tumor cells via the micropinocytosis and caveolin-mediated endocytosis pathway, followed by specific binding with cysteine-rich GA proteins via the disulfide bonds in thiopeptide assemblies (Figure 8f). Overloaded thiopeptide assemblies in the GA can effectively kill cancer cells. Moreover, replacing the NBD group with a Nap group to enhance the self-assembly process further decreased the IC$_{50}$ of probe **24** against HeLa tumor cells to 2.8 μM (Figure 8g,h).

Very recently, Wang and co-workers reported the MMP-2-responsive bispecific glycopeptide E-MISA probe **25** (bsGP) that simultaneously targeted CD206 on tumor-associated macrophages (TAMs) and CXCR4 on tumor cells, enabling regulation of the tumor microenvironment (TME) and inhibition of bladder cancer recurrence.[78] Probe **25** contained three mannoses for specific targeting and modulating TAMs, a CXCR4-specific bound peptide LGASWHRPDK, an MMP-2-specific recognized substrate PLGYLG peptide linker, and a hydrophobic peptide KLVFFAECG for molecular self-assembly (Figure 8i). Following i.v. injection of probe **25** into mice with an orthotopic EJ bladder tumor, it could rapidly diffuse and accumulate in the tumor tissues. They showed that probe **25** could efficiently target the M2-like TAMs in tumor tissues, repolarize them to the M1 phenotype, and subsequently increase the recruitment of CD8$^+$ T cells, potently remodeling the immunosuppressive TME. Moreover, within the tumor region, probe **25** could be cleaved by MMP-2, resulting in the release of the tumor-targeting CXCR4 residue. These released residues spontaneously self-assembled into nanofibers (**25**-NFs) that specifically bound to and sustainably arrested CXCR4 signaling in bladder tumor cells. This process could reduce tumor fibrosis and facilitate T cell infiltration, ultimately leading to a decrease in the recurrence of orthotopic bladder cancer (Figure 8j). In vivo NIR FLI showed that the NIR cyanine dye-containing bispecific glycopeptide probe **25**-Cy had more accumulation and retention in the EJ tumor tissues compared to the control probe (Pep$_{CXCR4}$), which merely targeted CXC4 (Figure 8k). The immunofluorescence staining results further confirmed that probe **25** could be cleaved by MMP-2 and self-assembled into **25**-NFs, which sustainably inhibited CXC4 signaling. Consequently, this led to downregulation of the phosphorylation levels of Erk and Akt,
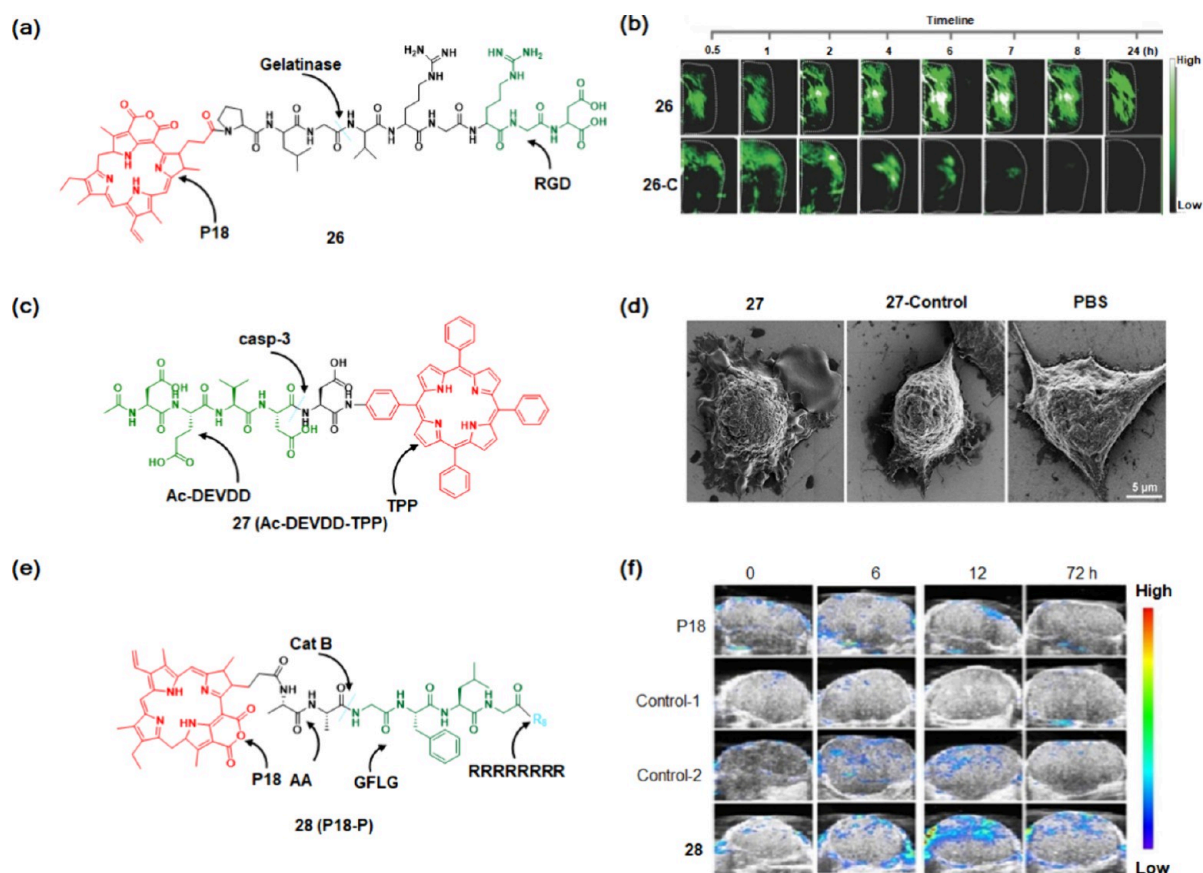
Figure 9. E-MISA theranostic probes for phototherapy and SDT. (a) Chemical structure of E-MISA theranostic probe **26** for PTT in vivo. (b) Representative PA images of U87 tumors that received i.v. injection of probe **26** or its control probe **26-C** (no RGD ligand) (200 μM, 200 μL) from 0.5 to 24 h. (c) Chemical structure of E-MISA theranostic probe **27** for PDT in vivo. (d) SEM images captured from SCC7 cells that were pretreated with cisplatin and then incubated with 10 μM probe **27**, **27-Control** (Ac-DEDVD-TPP), or PBS for 4 h, followed by irradiation with a 660 nm laser (6 mW cm^{-2}, 5 min). (e) Chemical structure of E-MISA probe **28** for SDT in vivo. (f) Representative PA images (λ_{ex} = 808 nm) of the tumor region after i.v. injection of probe **28**, Control-1 (P18-AAGF), Control-2 (P18-AAR$_8$), and free P18. Reproduced with permission from refs 165, 107, and 110. Copyright 2015 Wiley-VCH, 2023 American Chemical Society, and 2024 American Chemical Society, respectively.

thereby inhibiting bladder tumor growth and migration in mice (Figure 8l)

4.2. E-MISA Theranostic Probes for Phototherapy and/or SDT

Phototherapy (e.g., PTT and PDT) has shown promise in the treatment of superficial tumors because of the high spatiotemporal capacity of light, which allows for precise tumor therapy and reduces toxic side effects.[161−164] In 2015, Wang and colleagues developed the gelatinase-activatable E-MISA theranostic probe **26** for PAI-guided PTT of tumors in vivo.[165] Probe **26** comprised a hydrophobic porphyrin (P18) as the NIR PTT agent, a gelatinase-responsive PLGVRG substrate linker peptide, and a hydrophilic tumor-targeting peptide RGD ligand (Figure 9a). Following i.v. injection of probe **26** into U87-xenografted tumor-bearing mice, it actively targeted and enhanced accumulation at tumor tissue with the RGD ligand. In tumor tissues positive for gelatinase, the PLGVRG peptide of probe **26** was cleaved, releasing the hydrophobic P18−PLG fragment. This fragment spontaneously underwent in situ self-assembly into PA signal-enhanced P18-containing nanofibers (P18-NFs), resulting in strong PAI signals observed in tumor foci of the probe **25**-treated group (Figure 9b). Guided by PAI signals, an NIR laser (λ_{ex} = 730 nm; 150 mW) was applied 6 and 10 h after injection of probe **25**, achieving effective PTT of U87 tumors.

In addition to PTT, Liang and colleagues recently designed E-MISA theranostic probe **27** for oral tumor therapy by combining PDT with a casp-3-responsive self-amplification process.[107] Probe **27** (Ac-DEVDD-TPP) consisted of an Ac-DEVD substrate peptide for specific cleavage by casp-3 and an NIR tetraphenylporphyrin (TPP) derivative photosensitizer (PS) for PDT (Figure 9c). Upon submucosal injection of probe **27** into cisplatin-pretreated orthotopic SCC7 oral tumor-bearing mice, it was rapidly cleaved by casp-3 activated by cisplatin, resulting in the formation of hydrophobic D-TPP. D-TPP spontaneously self-assembled into TPP-containing nanofibers (**27**-NFs) and accumulated around the mitochondria of tumor cells. Guided by the NIR FLI signals, a 660 nm laser (6 mW cm^{-2}) was applied, leading to the production of cytotoxic singlet oxygen ($^1O_2$) by **27**-NFs, which induced deeper apoptosis and simultaneously increased the activation of more casp-3, further amplifying the apoptosis assembly process. Moreover, the authors found that this cyclic amplification mechanism could also significantly induce the pyroptosis process in cancer cells. Several pyroptosis process events were directly observed via scanning electron microscopy (SEM) images of the probe **27**-treated SCC7 tumor cells (Figure 9d). Furthermore, this cyclic amplification strategy significantly inhibited the growth of orthotopic SCC7 oral
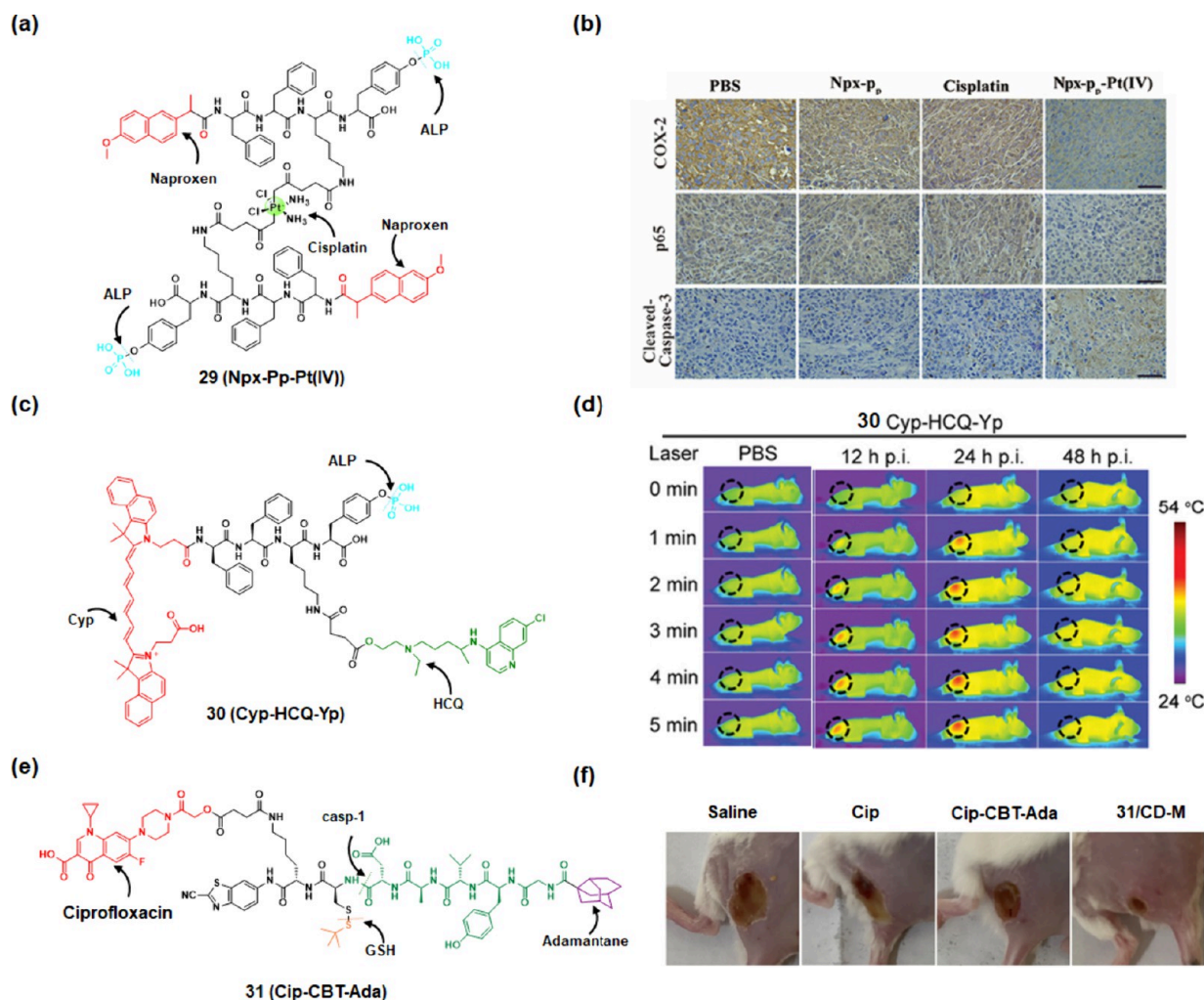
Figure 10. E-MISA probes for combination therapy or antibacterial infection. (a) Chemical structure of probe **29** for chemodrug/resistance inhibitor combination therapy. (b) Representative immunofluorescence staining images of COX-2, p65, and cleaved casp-3 in tumor tissues with indicated treatment of HeLa tumor-bearing mice. Scale bar: 100 μm. (c) Chemical structure of probe **30** for PTT/autophagy inhibitor combination therapy. (d) Representative thermal images of HepG2 tumor-bearing mice that received i.v. injection of PBS or probe **30**. Images were captured before (0 min) or after (1−5 min) irradiation with an 808 nm NIR laser (0.3 W cm^{-2}). (e) Chemical structure of probe **31** for anti-*S. aureus* infection therapy. (f) Representative images of *S. aureus*-infected mice at day 3 with different treatments. Reproduced with permission from refs 86, 87, and 169. Copyright 2021, 2021, and 2023 Wiley-VCH, respectively.

tumors in mice in the probe **27** + cisplatin + laser-treated group for up to 30 days.

SDT, with a higher penetration capability than phototherapy, is a highly promising method in modern therapy tools. However, the low bioavailability and accumulation of the sonosensitizers have hindered the outcomes. Recently, Liu and co-workers utilized the E-MISA strategy and designed the cat B-responsive probe **28** (P18-P) for SDT of tumors in vivo.[110] Probe **28** comprised an R_8 (RRRRRRRR) cell-penetrating peptide to enhance the entrance capability into tumor cells, a substrate linker peptide (GFLG) for specific cleavage by cat B, a self-assembly structural motif peptide (AA), and a porphyrin-based derivative P18 for PAI and SDT (Figure 9e). Following i.v. injection of probe **28** into s.c. HepG2 tumor-bearing mice, it deeply diffused into tumor tissues. The cell-penetrating R_8 peptide increased the tumor cells internalization of probe **28**. Once probe **28** entered tumor cells, the cat B-triggered in situ self-assembly process was initiated, resulting in the generation of substantial PA signal enhancement P18-containing nanoparticles (**28**-NPs) in the tumor region. Due to the enhanced

accumulation and retention of **28**-NPs, strong PAI signals were observed in the tumor region (Figure 9f). Guided by the PAI signal, ultrasound irradiation (1 mHz, 0.97 W/cm^2, 5 min, 40% cycle) was applied, boosting reactive oxygen species (ROS) generation and improving SDT efficacy in vivo.

4.3. E-MISA Theranostic Probes for Combination Therapy

Combination therapy, which involves the use of two or several therapeutics for the treatment, has demonstrated significant advantages over monotherapy, particularly in overcoming drug resistance and improving treatment outcomes.[166−168] In 2021, Liu and co-workers reported the ALP-responsive E-MISA probe **29** (Npx-Pp-Pt(IV)) for combination therapy of tumors.[86] Probe **29** comprised two ALP-recognition hydrophobic Phe-Phe-Tyr(H$_2$PO$_3$) tripeptides for self-assembly; two nonsteroidal anti-inflammatory drug (naproxen, Npx) molecules to suppress the cyclooxygenase-2 (COX-2)-related pathway, which was associated with cisplatin resistance; and a GSH-responsive cisplatin prodrug Pt(IV) linker (Figure 10a). Following i.v. injection of probe **29** into ALP-overexpressing HeLa tumor-bearing mice, it rapidly diffused
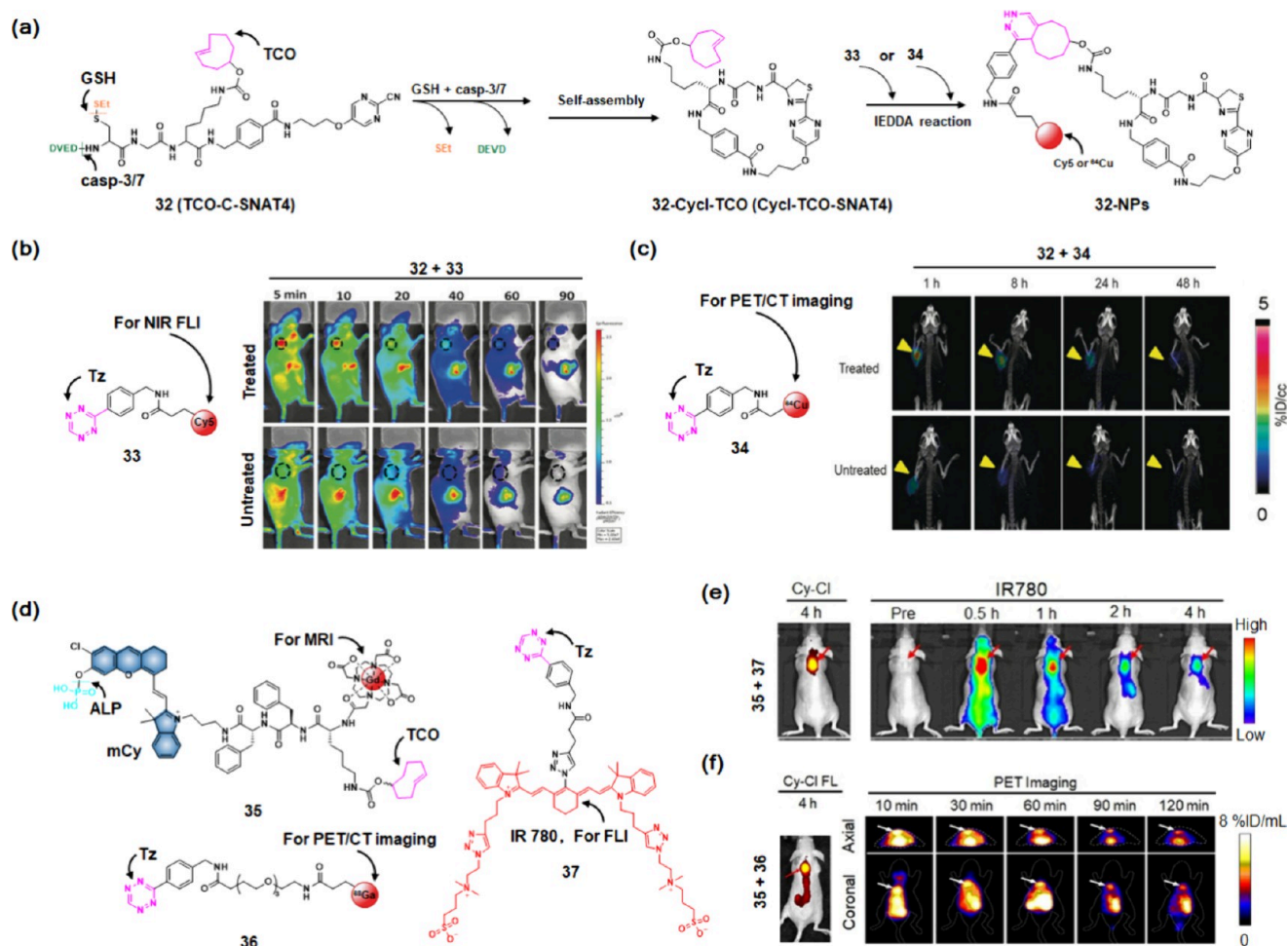
Figure 11. Integration of the E-MISA process with the IEDDA reaction for pretargeted imaging. (a) Chemical structure of probe **32** and the proposed pretargeted imaging using the E-MISA strategy and the bioorthogonal IEDDA reaction. (b) Chemical structure of probe **33** and the longitudinal fluorescence imaging of (top) drug-treated (10 μM cisplatin) and (bottom) untreated 460 tumor-bearing mice following i.t. injection with probe **32** (10 nmol) and i.v. injection with probe **33** (5 nmol) after 30 min. The images were captured 5−90 min after injection of probe **33**. (c) Chemical structure of probe **34** and PET imaging of nude mice with (top) cisplatin-treated and (bottom) untreated H460 tumor at 1, 8, 24, and 48 h. Mice received i.t. injection of probe **32** (5 nmol) followed by i.v. injection of **34** (ca. 400 mCi). (d) Chemical structures of E-MISA probes **35**, **36**, and **37** for pretargeted imaging in vivo. (e, f) Longitudinal FL imaging (IR 780) and (f) PET imaging of HeLa tumor-bearing mice receiving i.v. injection of probe **37** (25 μM, 200 μL) at 0 (pre), 0.5, 1, 2, and 4 h or i.v. injection of probe **36** (∼7.4 MBq) at 10, 30, 60, 90, and 120 min, respectively. Before injection of probe **37** or **36**, probe **35** (50 μM) was pretreated at 4 h, and the FL images (Cy-Cl) were captured at 4 h after the indicated injection. Reproduced with permission from refs 108 and 88. Copyright 2020 and 2021 Wiley-VCH, respectively.

into the tumor site and initiated the subsequent ALP-triggered in situ self-assembly process. This process enhanced the accumulation and retention of cisplatin-containing nanofibers (**29**-NFs) in the tumor region. Once the **29**-NFs were internalized by tumor cells, the cisplatin prodrug Pt(IV) could be reduced by GSH, transforming into Pt(II) to produce chemotherapy efficacy. Simultaneously, the Npx in **29**-NFs could suppress the COX-2-related pathways, thereby alleviating activation of the cisplatin-resistance-related pathways and enhancing the combination therapy efficacy of tumors. The authors demonstrated that probe **29**-treated tumor-bearing mice exhibited decreased levels of COX-2 expression. This decrease in the level of COX-2 expression further inhibited NF-κB expression (p-p65, a major component of NF-κB) and promoted the levels of cleaved casp-3 expression (Figure 10b). These changes collectively enhanced the efficacy of combination therapy in vivo.

In addition to using chemodrugs and resistance inhibitors in the E-MISA probe for combination therapy, the incorporation

of the autophagy inhibition drug hydroxychloroquine (HCQ) with PTT could also achieve combination therapy efficacy. Based on this concept, in 2021 Liang and co-workers reported the E-MISA theranostic probe **30** (Cyp-HCQ-Yp) for mild-temperature PTT of tumors.[87] Probe **30** comprised an ALP-recognition hydrophobic Phe-Phe-Lys-Tyr(H₂PO₃) tetrapeptide for self-assembly, the carboxylesterase (CES)-responsive autophagy inhibitor HCQ, and the NIR dye cypate as a PTT agent and promoter of self-assembly (Figure 10c). Following i.v. injection of probe **30** into ALP- and CES-overexpressing HepG2 tumor-bearing mice, the probe could easily diffuse into the tumor site and proceed via an ALP-triggered dephosphorylation process. This process could generate tumor-membrane-anchored CyP-HCQ-Y, beneficially enhancing tumor cell uptake of CyP-HCQ-Y. Once the Cyp-HCQ-Y was internalized by tumor cells, it could be further cleaved by intracellular CES, leading to release of Cyp-Y and HCQ. The released Cyp-Y spontaneously self-assembled into photothermal-enhanced Cyp-containing nanoparticles (**30**-NPs) in the tumor region.
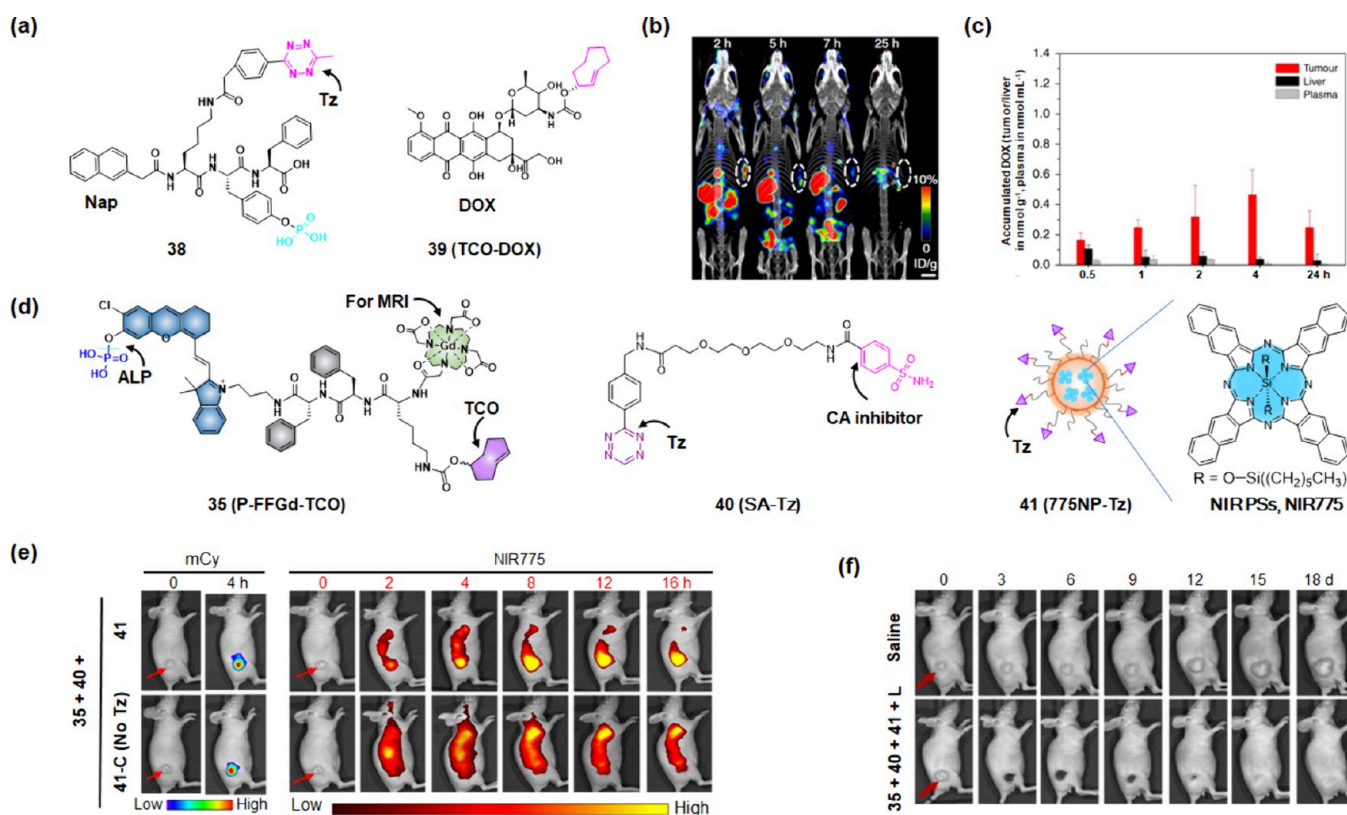
Figure 12. E-MISA strategy with IEDDA reaction for pretargeted therapeutics in vivo. (a) Chemical structures of probes **38** and **39**. (b) Representative SPECT/CT images of i.v. coinjection of probe **38** (50 mg kg^{-1}) and its ^{125}I-labeled probe **38**-^{125}I (0.875 mg kg^{-1}, 700 μCi) at different time points postinjection. The white dotted circles indicate the tumor region. (c) UPLC-MS/MS analysis of activated DOX in the tumor, liver, and plasma after i.v. injection of probe **38** (50 mg kg^{-1}) followed by i.v. injection of probe **39** (30 mg kg^{-1}) after a 2 h interval ($n = 5$). (d) Chemical structures of probes **35**, **40**, and **41** and NIR dye NIR 775. (e) Longitudinal FL imaging (NIR 775) of HeLa tumor-bearing mice receiving i.v. injection of probe **40/41** (4/1, 25 μM in total) at 0 (pre), 2, 4, 8, 12, and 16 h. Before injection of probes **40/41**, probe **35** (50 μM) was pretreated at 4 h, and the FL images (mCy) were captured before (0 h) and 4 h after indicated injection. (f) Photographs of s.c. HeLa tumors in living mice upon indicated treatments. Mice with s.c. HeLa tumors were i.v. injected with saline (200 μL) or probe **35** (1.0 mM, 200 μL). After 4 h, probes **40/41** (1/4, 250 μM, 200 μL) were i.v. injected, followed by irradiation with the 808 nm laser (0.33 W cm^{-2}, 10 min) at 12 h. Reproduced with permission from ref 89 (CC BY 4.0) and 90 (copyright 2023 Wiley-VCH).

Upon irradiation with NIR light (808 nm, 0.3 W cm^{-2}, 5 min), enhanced PTT effects were produced in the tumor region. Meanwhile, with the released HCQ within tumor cells, the autophagy process was inhibited, and the thermoresistance of tumor cells was decreased. Consequently, the PTT efficacy of probe **30** was enhanced. The in vivo data validated that the dual-enzyme-controlled E-MISA probe **30** significantly enhanced thermal signals and simultaneously inhibited the autophagy process to enhance mild-temperature PTT efficacy in HepG2 tumors (Figure 10d).

The E-MISA strategy could also be utilized to precisely guide antibiotics to eliminate intracellular *Staphylococcos aureus* infection in vivo. Liang and co-workers recently designed the adamantane (Ada)-containing antibiotic-peptide E-MISA probe **31** (Cip-CBT-Ada) for tandem guest−host receptor recognitions to precisely guide ciprofloxacin (Cip) elimination of intracellular *S. aureus*.[169] Probe **31** consisted of an antibiotic Cip drug for elimination of bacteria infection, a CBT−Cys scaffold, a cap-1-responsive Tyr-Val-Ala-Asp substrate peptide, and an Ada guest for specific recognition with its host *β*-cyclodextrin-heptamannoside (CD-M) (Figure 10e). They utilized the guest−host recognition force between probe **31** containing the Ada guest and the CD-M host to yield **31/CD-M** (Cip-CBT-Ada/CD-M). Following s.c. injection of **31/CD-M** into *S. aureus*-infected mice, it specifically targets the

infected foci macrophage surface's mannose receptor via multivalent ligand−receptor recognition, promoting the internalization of **31/CD-M** by the macrophage cells. Due to both the presences of GSH and casp-1 in *S. aureus*-infected macrophages, the S-*t*-Bu-group and Tyr-Val-Ala-Asp substrate peptide were removed. Subsequently, the biocompatible condensation reaction triggers a self-assembly process and transforms into Cip-containing nanoparticles (**31**-NPs) trapped within the *S. aureus*-infected macrophages to eliminate intracellular *S. aureus* infection. The authors demonstrated that **31/CD-M** could effectively eliminate the *S. aureus* bacteria and prevent further development of infection, significantly decreasing the infected tissue area observed in **31/CD-M**-treated mice (Figure 10f). In the future, more antibacterial infection E-MISA strategies could be designed for various enzymes that are highly expressed on bacterial infected regions.[170]

5. E-MISA PROBES FOR PRETARGETED IMAGING AND THERANOSTICS OF TUMORS

The E-MISA strategy, due to its significant enhancement of functional nanoaggregate accumulation and retention in specific regions of interest, has prompted researchers to consider the potential utility of these accumulated nano-

aggregates as "artificial receptors". Leveraging these nano-aggregates combined with other functional molecules via bioorthogonal reactions, pretargeted imaging and/or thera-nostics in vivo can be achieved.[171−173] Based on this idea and the concept, Rao's group leveraged the optimized biocompat-ible intramolecular macrocyclization reaction between pyr-imidinecarbonitrile and D-Cys with the inverse-electron-demand Diels−Alder (IEDDA) reaction between tetrazine (Tz) and *trans*-cyclooctene (TCO) and developed the E-MISA probe **32** for protease activity multimodality imaging in vivo in 2020.[108] Probe **32** (TCO-C-SNAT 4) contained a TCO handle for rapid reaction with Tz tags (**33** and **34**) via the IEDDA reaction, a casp-3/7-responsive DEVD substrate peptide, and a GSH reduction disulfide bond. Upon cleavage by casp-3 and reduction by GSH, probe **32** underwent an intramolecular macrocyclization reaction and in situ self-assembled into TCO-handle-containing nanoparticles (**32**NPs-TCO, Cycl-TCO-SNAT4). **32**NPs-TCO rapidly captured Tz-bearing imaging tags via the fast IEDDA reaction, forming Cy5- or ^{64}Cu-containing nanoparticles (**32**-NPs) for NIR FLI or PET in vivo (Figure 11a). Following i.t. injection of probe **32** into cisplatin-treated H460 tumor-bearing mice, it under-went conversion into **32**NPs-TCO in apoptotic tumor tissues via casp-3/7 and GSH-reduced intramolecular macrocycliza-tion and a self-assembly process. Subsequent i.v. injection of Tz tag probe **33** or **34** resulted in significant enhancement of NIR FL or a strong PET signal in cisplatin-treated H460 tumor-bearing mice, respectively. Moreover, this E-MISA pretargeting strategy significantly enhanced the accumulation of imaging tags in the tumor region, with NIR FL lasting for 100 min, and the PET imaging signal retention for up to 2 days in the tumor region (Figure 11b,c).

Based on this cascade E-MISA strategy and IEDDA reaction, Ye and colleagues established an activatable pretargeted approach for NIR FL/MRI/PET multimodal imaging of ALP activity in vivo.[88] Based on the structure of probe **14**, they further introduced a lysine residue decorated with a TCO handle into probe **14** and designed probe **35** (P-FFGd-TCO) to enable the bioorthogonal IEDDA reaction (Figure 11d). Following i.v. injection of E-MISA probe **35** into HeLa tumor-bearing mice, the probe **35** was extravasated and penetrated into the tumor tissues due to the small molecule and hydrophilic capabilities. Once dephosphorylated by the overexpressed ALP on the tumor membrane, probe **35** underwent rapid in situ self-assembly and transformed into TCO-containing nanoparticles with NIR FL and MRI signals both increased. A large number of TCO-bearing nanoparticles ($>10^9$ TCO per cell) could anchor on the tumor surface, which could serve as "artificial antigens" to bypass the limited number of natural antigens on a single tumor cell ($\sim10^6$ per cell).[174,175] After i.v. injection of fluorescent IR780-labeled Tz tag (**37**) or radioactive ^{68}Ga-labeled Tz tag (**36**), the membrane-residing "artificial antigens" permitted the substantial capture of the Tz tags through the rapid IEDDA reaction between the TCO handles and the Tz tags. This increased the retention and accumulation of IR780 or the ^{68}Ga radioisotope at the tumor foci. Consequently, bright NIR FLI signals of IR780 or PET signals from [^{68}Ga] could be observed in the probe **35**-pretreated group (Figure 11e,f).

In addition to using E-MISA with a pretargeted strategy for molecular imaging, researchers have explored its application for drug release or therapy in vivo. In 2018, Gao and co-workers reported the ALP-responsive E-MISA probe **38** with Tz/TCO

bioorthogonal decaging reaction to trigger the activation and release of a DOX prodrug in vivo (Figure 12a).[89] Probe **38** comprised a Nap group to enhance the self-assembly, an ALP-responsive Lys-Tyr(H_2PO_3)-Phe tripeptide linker, and a Tz handle for the IEDDA bioorthogonal reaction. Following i.v. coinjection of **38** and its ^{125}I-labeled probe **38**-^{125}**I** into ALP-overexpressing s.c. HeLa tumor-bearing mice, strong single-photon emission computed tomography/computed tomogra-phy (SPECT/CT) imaging signals were observed in the tumor region at 2 h, indicating the accumulation of dephosphorylated products of probe **38** at the tumor site (Figure 12b). Following i.v. injection of the DOX prodrug probe **39** (TCO−DOX), TCO−DOX was activated and released DOX in tumor foci via the IEDDA decaging reaction, resulting in effective chemo-therapy in the tumor region (Figure 12c).

By leveraging the E-SIMA strategy with the IEDDA reaction, concurrent enrichment of two therapeutic agents for synergistic tumor therapy in vivo could also be achieved. Ye's group recently integrated their previously reported E-MISA probe **35** for pretargeted dual-channel NIR FL (710 and 780 nm)/MRI bimodal imaging-guided synergistic PDT in vivo (Figure 12d).[90] They synthesized two new Tz-tagged therapeutic agents, including **40** (a small-molecule carbonic anhydrase (CA) inhibitor) and **41** (an NIR PS-encapsulated nanoparticle). Following i.v. injection of **35** into HeLa tumor-bearing mice, a large amount of NIR FLI (mCy)/MRI signals-enhanced TCO-containing nanoparticles (**35**NPs-TCO) were observed in the tumor region, resulting from the ALP-triggered in situ self-assembly process. Concurrently, i.v. injection of probes **40** and **41** led to more pronounced NIR FLI of NIR775 in the tumor region of the probe **41**-treated mice compared to the control (no Tz tag) probe **41**-**C**-treated mice. The results indicated that E-MISA with the IEDDA bioorthogonal strategy could trap and enhance the accumulation of more NIR PSs in tumor tissues than the approach that solely relied on the enhanced permeability and retention (EPR) effect to enhance the accumulation of PSs in tumor tissues (Figure 12e). Furthermore, the IEDDA reaction between probe **35**, **40**, and **41** induced the regrowth of nanoparticles (**35**-NPs-TCO) and their transformation into multifunctional microparticles (FMNPs-775/SA) trapped in the tumor region. The long-time residue of FMNPs-775/SA could sustainably inhibit the activity of CA, alleviating the hypoxic environment of tumors. Consequently, this significantly enhanced the synergistic PDT of hypoxic tumors. The anticancer results demonstrated that s.c. HeLa tumors (~200 mm^3) were completely eradicated without recurrence after a single 10 min session of 808 nm laser (0.33 W cm^{-2}) irradiation (Figure 12f). This strategy holds potential as a general approach for the simultaneous accumulation of other therapeutic drug molecules, achieving synergistic therapy of tumors.

6. CONCLUSIONS AND OUTLOOK

In this Perspective, we have summarized the design principles and construction strategies of E-MISA probes, focusing on their applications in molecular imaging and/or theranostics in vivo. We have primarily focused on the recent advances in the development of different E-MISA probes for in vivo imaging and theranostics of tumors by targeting extracellular or intracellular enzymes. The E-MISA probes have the following advantages for in vivo imaging and/or theranostics. The E-MISA strategy utilizes small-molecule probes, which have deep tissue penetration ability. The small size of the E-MISA probes

allows for rapid extravasation and penetration into tumor tissues after systemic administration. Subsequently, they can undergo the E-MISA process and transform into nano-aggregates in the tumor regions. These large-size nano-aggregates have reduced diffusion compared to the small-molecule precursors, benefiting prolonged retention and enhanced accumulation of molecular agents or therapeutic agents in the tumor tissues. This results in high signal to background ratio (SBR) imaging signals or enhanced anticancer efficacy in vivo.[82,105] Also, E-MISA enables multimodal imaging and/or combination therapy effects in vivo. The multimodality imaging E-MISA probes serve as powerful tools for achieving more accurate and comprehensive imaging of enzyme activity in vivo. The sustained catalytic activity of enzymes facilitates the accumulation of numerous imaging functional molecules in tumor tissues, thereby addressing the requirements of MRI, which necessitates a high tissue penetration depth but with low sensitivity. Consequently, the combination of highly sensitive FLI with MRI can furnish high sensitivity and deep tissue imaging information in vivo, thereby facilitating precise preoperative diagnosis and intraoperative tumor resection via a bimodality-imaging-guided process.[80] Therefore, the use of E-MISA multimodality imaging probes is advantageous in providing molecular information on a target enzyme in vivo. In terms of therapy, the E-MISA strategy enables the accumulation of a large number of multifunctional therapeutic molecules in tumor tissues, achieving synergistic therapeutic effects. For instance, the combination of the PTT agent Cyp with the autophagy inhibitor CHQ enhanced the mild-temperature PTT efficacy for HepG2 tumor-bearing mice.[87] Additionally, the small size of E-MISA theranostic probes allows for rapid clearance from nonspecific regions and evasion of RES trapping, thereby reducing the risk of systemic side effects; E-MISA combined with pretargeted strategies enables the reassembly of nanoparticles and the modification of functional molecules in vivo. By capitalizing on the accumulation and retention ability of E-MISA probes to gather a large quantity of functional nanoaggregates in tumor tissues, the incorporation of bioorthogonal moieties into E-MISA probes facilitates the targeted installation of artificial functional nanoaggregates in tumor tissues. With the highly effective and sustained catalytic activity of enzymes, the accumulated bioorthogonal moieties far surpass the number of known natural antigens. Consequently, by utilizing these bioorthogonal functional-group-containing nanoaggregates as artificial antigens, subsequent large-scale trapping of imaging or therapeutic functional molecules containing bioorthogonal tags occurs rapidly through bioorthogonal reactions upon reaching the tumor tissue. This process permits reassembly and modification of functional molecules at the tumor site, achieving multimodality imaging and/or synergistic therapeutic effects in vivo.[88,90]

In the last decades, E-MISA molecular probes have made significant advancements in molecular imaging and theranostics. However, this field still faces several challenges. (1) Precise control of the size, morphology, and functionality of E-MISA probes in vivo presents a formidable challenge. Manipulating the size, morphology, and functionality of the E-MISA process to generate aggregates within the highly dynamic and complex environment of living organisms remains challenging. It is possible to precisely control the size, morphology, and functionality of E-MISA probes by designing novel dyes or peptide molecules or integrating other reactions or forces to fine-tune the self-assembly process. (2) The E-MISA probes are subject to limitations due to their short blood circulation time and rapid clearance in vivo. This results in a significant reduction in their bioavailability in living subjects. The use of polymer structures to modulate the probes' size, charge, and hydrophilicity/hydrophobicity may offer a promising approach to addressing the limitations of small-molecule pharmacokinetics in vivo and maintaining strong tissue penetration. (3) Effective translocation into cells for efficient intracellular E-MISA process must be improved. Enhancing the cell-penetrating ability of E-MISA probes is crucial for improving intracellular enzyme (furin or casp) activation responses in the E-MISA process. Strategies involving alterations in the tumor extracellular microenvironment or enzyme-responsive charge conversion could significantly increase the probe uptake by converting small molecules originally with negative or neutral charge into positively charged molecules. (4) The specificity of the E-MISA strategy can be improved. It is evident that certain enzyme expression sites are not exclusively within the designated sites in biological organisms. For instance, GGT and ALP have low levels in the blood,[176] whereas MMPs are released from MMP-over-expressing tumors into the blood. The presence of enzymes in the blood may contribute to elevated background signals, reduction of the SBR, or even production of adverse effects in vivo.[177] To address this issue, the use of bienzyme- or multienzyme-activatable E-MISA probes may prove to be an effective strategy for reducing nonspecific background signals and enhancing imaging and/or therapeutic effects in vivo.[178]

In the future, the development of E-MISA is expected to exhibit a more diverse, precise, and clinical trend. Diversity is reflected in applying the E-MISA strategy with other controlled, rapid, accurate release methods (such as pH, GSH, ROS, light, US, etc.) or leveraging other bioorthogonal reactions (such as azide click reaction,[179] IEDDA reaction, CBT–Cys reaction, etc.) to concurrently accumulate various functional components (such as toxins,[180] radioactive drugs,[181] STING agonists,[182] immune vaccines,[183] etc.) at the tumor site. This could establish some versatile diagnostic and therapeutic platforms for various disease therapies in vivo and extend precise control of the E-MISA process to subcellular organelle structures. The regulation of the E-MISA strategy to the refined and enclosed subcellular organelle structures could exploit the advantages of nanoaggregates, such as prolonged residence time and multibinding site forces, to facilitate intervention, regulation, or even disruption of the organelle functions or behaviors. This could facilitate the regulation of the entire cell, tissue, and even the entire biological system. Clinical application of the E-MISA strategy has demonstrated its potential for precise imaging-guided surgical resection and achieving synergistic therapy under imaging guidance. It is of paramount importance to reduce potential toxicity effects, such as potential long-term retention toxicity, off-target toxicity, or immune responses from E-MISA probes or transformed nanoaggregates in clinical settings. One potential solution is to select some biocompatible and degradable organic materials to minimize the toxicity effects of E-MISA probes. Nevertheless, note that some organic fluorophores present in E-MISA probes are unable to degrade in vivo. It is therefore of the utmost importance to consider the controlled disassembly of these materials and to facilitate their clearance from the human body once they have fulfilled their imaging or therapeutic functions in vivo. Some E-MISA probes

are cleared predominantly via the hepatic pathway because the probes' fluorophores bind with proteins in the blood, thus forming larger-size complexes. This results in the probes being trapped by the RES and accumulated by the liver, which metabolizes only via the hepatic system. The hepatic clearance system exhibited a clearance rate that was considerably lower than that of the kidney clearance system, which could increase the potential for toxicity risks in vivo.[29,184] Consequently, the hydrophilic unbound protein and controllable degradable E-MISA probes present a more promising avenue for future clinical applications.

Therefore, developing smart E-MISA probes is imperative to tackle the challenges and potential issues mentioned earlier. This Perspective is expected to provide some guidance for creating novel methods, imaging agents, and theranostic probes using the E-MISA strategy. Future advancements are expected to generate more E-MISA probes with smart functionalized properties. These probes are anticipated to play a pivotal role in the fields of chemistry, biology, and medicine.

■ AUTHOR INFORMATION

Corresponding Authors

Deju Ye − State Key Laboratory of Analytical Chemistry for Life Science, Chemistry and Biomedicine Innovation Center (ChemBIC), School of Chemistry and Chemical Engineering, Nanjing University, Nanjing 210023, China; ● orcid.org/0000-0002-9887-0914; Email: dejuye@nju.edu.cn

Jian He − Department of Nuclear Medicine, Nanjing Drum Tower Hospital, Affiliated Hospital of Medical School, Nanjing University, Nanjing 210008, China; Email: hjxueren@126.com

Authors

Xidan Wen − Department of Nuclear Medicine, Nanjing Drum Tower Hospital, Affiliated Hospital of Medical School, Nanjing University, Nanjing 210008, China; State Key Laboratory of Analytical Chemistry for Life Science, Chemistry and Biomedicine Innovation Center (ChemBIC), School of Chemistry and Chemical Engineering, Nanjing University, Nanjing 210023, China

Chao Zhang − Department of Neurosurgery, Zhujiang Hospital, Southern Medical University, Guangzhou 510282, China

Yuyang Tian − State Key Laboratory of Analytical Chemistry for Life Science, Chemistry and Biomedicine Innovation Center (ChemBIC), School of Chemistry and Chemical Engineering, Nanjing University, Nanjing 210023, China

Yinxing Miao − State Key Laboratory of Analytical Chemistry for Life Science, Chemistry and Biomedicine Innovation Center (ChemBIC), School of Chemistry and Chemical Engineering, Nanjing University, Nanjing 210023, China

Shaohai Liu − State Key Laboratory of Analytical Chemistry for Life Science, Chemistry and Biomedicine Innovation Center (ChemBIC), School of Chemistry and Chemical Engineering, Nanjing University, Nanjing 210023, China

Jing-Juan Xu − State Key Laboratory of Analytical Chemistry for Life Science, Chemistry and Biomedicine Innovation Center (ChemBIC), School of Chemistry and Chemical Engineering, Nanjing University, Nanjing 210023, China; ● orcid.org/0000-0001-9579-9318

Complete contact information is available at:
https://pubs.acs.org/10.1021/jacsau.4c00392

■ REFERENCES

(1) Capito, R. M.; Azevedo, H. S.; Velichko, Y. S.; Mata, A.; Stupp, S. I. Self-Assembly of Large and Small Molecules into Hierarchically Ordered Sacs and Membranes. *Science* **2008**, *319* (5871), 1812−1816.

(2) Baker, R. W.; Hughson, F. M. Chaperoning SNARE Assembly and Disassembly. *Nat. Rev. Mol. Cell Biol.* **2016**, *17* (8), 465−479.

(3) Jenkyn-Bedford, M.; Jones, M. L.; Baris, Y.; Labib, K. P. M.; Cannone, G.; Yeeles, J. T. P.; Deegan, T. D. A Conserved Mechanism for Regulating Replisome Disassembly in Eukaryotes. *Nature* **2021**, *600* (7890), 743−747.

(4) Abelein, A.; Ciofi-Baffoni, S.; Mörman, C.; Kumar, R.; Giachetti, A.; Piccioli, M.; Biverstal, H. Molecular Structure of Cu(II)-Bound Amyloid-β Monomer Implicated in Inhibition of Peptide Self-Assembly in Alzheimer's Disease. *JACS Au* **2022**, *2* (11), 2571−2584.

(5) Levin, A.; Hakala, T. A.; Schnaider, L.; Bernardes, G. J. L.; Gazit, E.; Knowles, T. P. J. Biomimetic Peptide Self-Assembly for Functional Materials. *Nat. Rev. Chem.* **2020**, *4* (11), 615−634.

(6) Shen, H.; Fallas, J. A.; Lynch, E.; Sheffler, W.; Parry, B.; Jannetty, N.; Decarreau, J.; Wagenbach, M.; Vicente, J. J.; Chen, J.; Wang, L.; Dowling, Q.; Oberdorfer, G.; Stewart, L.; Wordeman, L.; De Yoreo, J.; Jacobs-Wagner, C.; Kollman, J.; Baker, D. De Novo Design of Self-Assembling Helical Protein Filaments. *Science* **2018**, *362* (6415), 705−709.

(7) Versluis, F.; van Esch, J. H.; Eelkema, R. Synthetic Self-Assembled Materials in Biological Environments. *Adv. Mater.* **2016**, *28* (23), 4576−4592.

(8) Arancillo, M.; Taechalertpaisarn, J.; Liang, X.; Burgess, K. Piptides: New, Easily Accessible Chemotypes For Interactions With Biomolecules. *Angew. Chem., Int. Ed.* **2021**, *60* (12), 6653−6659.

(9) He, H.; Tan, W.; Guo, J.; Yi, M.; Shy, A. N.; Xu, B. Enzymatic Noncovalent Synthesis. *Chem. Rev.* **2020**, *120* (18), 9994−10078.

(10) Gao, J.; Zhan, J.; Yang, Z. Enzyme-Instructed Self-Assembly (EISA) and Hydrogelation of Peptides. *Adv. Mater.* **2020**, *32* (3), No. 1805798.

(11) Li, C. Y.; Liang, Z.; Liu, L.; Kuang, Y. Intracellular Molecules Induced Extracellular Peptide Self-Assembly for Efficient and Effective In Situ Cell Purification. *Angew. Chem., Int. Ed.* **2023**, *62* (37), No. e202306533.

(12) Deng, K.; Luo, Z.; Tan, L.; Quan, Z. Self-assembly of Anisotropic Nanoparticles into Functional Superstructures. *Chem. Soc. Rev.* **2020**, *49* (16), 6002−6038.

(13) Zhang, L.; Wang, X.; Zhao, J.; Sun, B.; Wang, W. Construction of Targeting-Peptide-Based Imaging Reagents and Their Application in Bioimaging. *Chem. Biomed. Imaging* **2024**, *2* (4), 233−249.

(14) Bera, S.; Basu, S.; Jana, B.; Dastidar, P. Real-time Observation of Macroscopic Helical Morphologies under Optical Microscope: A Curious Case of π−π Stacking Driven Molecular Self-assembly of an Organic Gelator Devoid of Hydrogen Bonding. *Angew. Chem., Int. Ed.* **2023**, *62* (7), No. e202216447.

(15) Wong, Y.-S.; Ng, M.; Yeung, M. C.-L.; Yam, V. W.-W. Platinum(II)-Based Host−Guest Coordination-Driven Supramolecu-

lar Co-Assembly Assisted by Pt···Pt and π−π Stacking Interactions: A Dual-Selective Luminescence Sensor for Cations and Anions. *J. Am. Chem. Soc.* **2021**, *143* (2), 973−982.

(16) Nandakumar, A.; Ito, Y.; Ueda, M. Solvent Effects on the Self-Assembly of an Amphiphilic Polypeptide Incorporating α-Helical Hydrophobic Blocks. *J. Am. Chem. Soc.* **2020**, *142* (50), 20994−21003.

(17) Judd, K. D.; Mendes de Oliveira, D.; Urbina, A. S.; Ben-Amotz, D. Influence of H⁺, OH⁻ and Salts on Hydrophobic Self-Assembly. *Chem. Sci.* **2024**, *15*, 6378−6384.

(18) Sherrington, D. C.; Taskinen, K. A. Self-Assembly in Synthetic Macromolecular Systems Multiple Hydrogen Bonding Interactions. *Chem. Soc. Rev.* **2001**, *30* (2), 83−93.

(19) Gallonde, W. T.; Poidevin, C.; Houard, F.; Caytan, E.; Dorcet, V.; Fihey, A.; Bernot, K.; Rigaut, S.; Galangau, O. Kinetic Delay in Cooperative Supramolecular Polymerization by Redefining the Trade-Off Relationship between H-Bonds and Van der Waals/π−π Stacking Interactions. *Angew. Chem., Int. Ed.* **2023**, *62* (49), No. e202313696.

(20) Zhu, Y.; Lai, H.; Gu, Y.; Wei, Z.; Chen, L.; Lai, X.; Han, L.; Tan, P.; Pu, M.; Xiao, F.; He, F.; Tian, L. The Balance Effect of π−π Electronic Coupling on NIR-II Emission and Photodynamic Properties of Highly Hydrophobic Conjugated Photosensitizers. *Adv. Sci.* **2024**, *11* (6), No. 2307569.

(21) Bi, Y.; Wang, Z.; Liu, T.; Sun, D.; Godbert, N.; Li, H.; Hao, J.; Xin, X. Supramolecular Chirality from Hierarchical Self-Assembly of Atomically Precise Silver Nanoclusters Induced by Secondary Metal Coordination. *ACS Nano* **2021**, *15* (10), 15910−15919.

(22) Rehm, T. H.; Schmuck, C. Ion-Pair Induced Self-Assembly in Aqueous Solvents. *Chem. Soc. Rev.* **2010**, *39* (10), 3597−3611.

(23) Wu, D.; Ni, C.; Lao, Z.; Cao, Y.; Ni, J.; Ren, Z.; Liu, S.; Tao, Y.; Xin, C.; Pan, D.; Hu, Y.; Chu, J. Temperature-Regulated Bidirectional Capillary Force Self-Assembly of Femtosecond Laser Printed Micropillars for Switchable Chiral Microstructures. *ACS Nano* **2023**, *17* (13), 12820−12828.

(24) Sun, X.; Yang, X.; Chen, Y.; Sun, J.; He, Z.; Zhang, S.; Luo, C. In Situ Self-Assembled Nanomedicines for Cancer Treatment. *Chem. Eng. J.* **2023**, *466*, No. 143365.

(25) Li, L.-L.; Qiao, Z.-Y.; Wang, L.; Wang, H. Programmable Construction of Peptide-Based Materials in Living Subjects: From Modular Design and Morphological Control to Theranostics. *Adv. Mater.* **2019**, *31* (45), No. 1804971.

(26) Kim, J.; Lee, S.; Kim, Y.; Choi, M.; Lee, I.; Kim, E.; Yoon, C. G.; Pu, K.; Kang, H.; Kim, J. S. In Situ Self-Assembly for Cancer Therapy and Imaging. *Nat. Rev. Mater.* **2023**, *8* (11), 710−725.

(27) Wang, Y.; Weng, J.; Wen, X.; Hu, Y.; Ye, D. Recent Advances in Stimuli-Responsive in Situ Self-Assembly of Small Molecule Probes for In Vivo Imaging of Enzymatic Activity. *Biomater. Sci.* **2021**, *9* (2), 406−421.

(28) Sawhney, R.; Jalan, R. The Gut is a Key Target of Therapy in Hepatic Encephalopathy. *Nat. Rev. Gastroenterol. Hepatol.* **2015**, *12* (1), 7−8.

(29) Cheng, P.; Pu, K. Molecular Imaging and Disease Theranostics with Renal-Clearable Optical Agents. *Nat. Rev. Mater.* **2021**, *6* (12), 1095−1113.

(30) Wang, X.; Pu, K. Molecular Substrates for the Construction of Afterglow Imaging Probes in Disease Diagnosis and Treatment. *Chem. Soc. Rev.* **2023**, *52* (14), 4549−4566.

(31) Li, Z.; Liang, P.-Z.; Xu, L.; Zhang, X.-X.; Li, K.; Wu, Q.; Lou, X.-F.; Ren, T.-B.; Yuan, L.; Zhang, X.-B. In Situ Orderly Self-Assembly Strategy Affording NIR-II-J-Aggregates for In Vivo Imaging and Surgical Navigation. *Nat. Commun.* **2023**, *14* (1), 1843.

(32) Qin, S.-Y.; Feng, J.-Q.; Cheng, Y.-J.; Liu, W.-L.; Zhang, A.-Q.; Wang, L.; Wang, H.; Zhang, X.-Z. A Comprehensive Review on Peptide-Bearing Biomaterials: From Ex Situ to In Situ Self-Assembly. *Coord. Chem. Rev.* **2024**, *502*, No. 215600.

(33) Yao, Q.; Huang, Z.; Liu, D.; Chen, J.; Gao, Y. Enzyme-Instructed Supramolecular Self-Assembly with Anticancer Activity. *Adv. Mater.* **2019**, *31* (45), No. 1804814.

(34) Sun, M.; Wang, C.; Lv, M.; Fan, Z.; Du, J. Intracellular Self-Assembly of Peptides to Induce Apoptosis against Drug-Resistant Melanoma. *J. Am. Chem. Soc.* **2022**, *144* (16), 7337−7345.

(35) Froimchuk, E.; Carey, S. T.; Edwards, C.; Jewell, C. M. Self-Assembly as a Molecular Strategy to Improve Immunotherapy. *Acc. Chem. Res.* **2020**, *53* (11), 2534−2545.

(36) Cong, Y.; Ji, L.; Gao, Y.-J.; Liu, F.-H.; Cheng, D.-B.; Hu, Z.; Qiao, Z.-Y.; Wang, H. Microenvironment-Induced In Situ Self-Assembly of Polymer−Peptide Conjugates That Attack Solid Tumors Deeply. *Angew. Chem., Int. Ed.* **2019**, *58* (14), 4632−4637.

(37) Hou, D.-Y.; Cheng, D.-B.; Zhang, N.-Y.; Wang, Z.-J.; Hu, X.-J.; Li, X.; Lv, M.-Y.; Li, X.-P.; Jian, L.-R.; Ma, J.-P.; Sun, T.; Qiao, Z.-Y.; Xu, W.; Wang, H. In Vivo Assembly Enhanced Binding Effect Augments Tumor Specific Ferroptosis Therapy. *Nat. Commun.* **2024**, *15* (1), 454.

(38) Cheng, D.-B.; Zhang, X.-H.; Gao, Y.-J.; Ji, L.; Hou, D.; Wang, Z.; Xu, W.; Qiao, Z.-Y.; Wang, H. Endogenous Reactive Oxygen Species-Triggered Morphology Transformation for Enhanced Cooperative Interaction with Mitochondria. *J. Am. Chem. Soc.* **2019**, *141* (18), 7235−7239.

(39) Li, Z.; Liang, P.-Z.; Ren, T.-B.; Yuan, L.; Zhang, X.-B. Orderly Self-Assembly of Organic Fluorophores for Sensing and Imaging. *Angew. Chem., Int. Ed.* **2023**, *62* (37), No. e202305742.

(40) Ye, D.; Pandit, P.; Kempen, P.; Lin, J.; Xiong, L.; Sinclair, R.; Rutt, B.; Rao, J. Redox-Triggered Self-Assembly of Gadolinium-Based MRI Probes for Sensing Reducing Environment. *Bioconjugate Chem.* **2014**, *25* (8), 1526−1536.

(41) Qiu, L.; Li, K.; Dong, W.; Seimbille, Y.; Liu, Q.; Gao, F.; Lin, J. Tumor Microenvironment Responsive "Head-to-Foot" Self-Assembly Nanoplatform for Positron Emission Tomography Imaging in Living Subjects. *ACS Nano* **2021**, *15* (11), 18250−18259.

(42) Jia, X.; Zhu, L. Photoexcitation-Induced Assembly: A Bottom-Up Physical Strategy for Driving Molecular Motion and Phase Evolution. *Acc. Chem. Res.* **2023**, *56* (6), 655−666.

(43) Yu, F.; Li, X.; Zhao, J.; Zhao, Y.; Li, L. Photoactivated DNA Assembly and Disassembly for On-Demand Activation and Termination of cGAS-STING Signaling. *Angew. Chem., Int. Ed.* **2023**, *62* (33), No. e202305837.

(44) Seo, J.; Khazi, M. I.; Bae, K.; Kim, J.-M. Temperature-Controlled Pathway Complexity in Self-Assembly of Perylene Diimide- Polydiacetylene Supramolecule. *Small* **2023**, *19* (18), No. 2206428.

(45) Basheer, A.; Shahid, S.; Kang, M. J.; Lee, J. H.; Lee, J. S.; Lim, D. W. Switchable Self-Assembly of Elastin- and Resilin-Based Block Copolypeptides with Converse Phase Transition Behaviors. *ACS Appl. Mater. Interfaces* **2021**, *13* (21), 24385−24400.

(46) Sang, Y.; Zhu, Q.; Zhou, X.; Jiang, Y.; Zhang, L.; Liu, M. Ultrasound-Directed Symmetry Breaking and Spin Filtering of Supramolecular Assemblies from only Achiral Building Blocks. *Angew. Chem., Int. Ed.* **2023**, *62* (8), No. e202215867.

(47) Cheng, D.-B.; Zhang, X.-H.; Chen, Y.; Chen, H.; Qiao, Z.-Y.; Wang, H. Ultrasound-Activated Cascade Effect for Synergistic Orthotopic Pancreatic Cancer Therapy. *iScience* **2020**, *23* (6), No. 101144.

(48) Feng, Z.; Han, X.; Wang, H.; Tang, T.; Xu, B. Enzyme-Instructed Peptide Assemblies Selectively Inhibit Bone Tumors. *Chem.* **2019**, *5* (9), 2442−2449.

(49) Liu, H.-W.; Chen, L.; Xu, C.; Li, Z.; Zhang, H.; Zhang, X.-B.; Tan, W. Recent progresses in small-molecule enzymatic fluorescent probes for cancer imaging. *Chem. Soc. Rev.* **2018**, *47* (18), 7140−7180.

(50) Guo, R.-C.; Zhang, X.-H.; Fan, P.-S.; Song, B.-L.; Li, Z.-X.; Duan, Z.-Y.; Qiao, Z.-Y.; Wang, H. In Vivo Self-Assembly Induced Cell Membrane Phase Separation for Improved Peptide Drug Internalization. *Angew. Chem., Int. Ed.* **2021**, *60* (47), 25128−25134.

(51) Wang, M.-D.; Lv, G.-T.; An, H.-W.; Zhang, N.-Y.; Wang, H. In Situ Self-Assembly of Bispecific Peptide for Cancer Immunotherapy. *Angew. Chem., Int. Ed.* **2022**, *61* (10), No. e202113649.

(52) Zhang, X.; Wang, J.; Zhang, Y.; Yang, Z.; Gao, J.; Gu, Z. Synthesizing biomaterials in living organisms. *Chem. Soc. Rev.* **2023**, *52* (23), 8126−8164.

(53) Lazcano, A. Prebiotic Evolution and Self-Assembly of Nucleic Acids. *ACS Nano* **2018**, *12* (10), 9643−9647.

(54) Hackett, S. R.; Zanotelli, V. R. T.; Xu, W.; Goya, J.; Park, J. O.; Perlman, D. H.; Gibney, P. A.; Botstein, D.; Storey, J. D.; Rabinowitz, J. D. Systems-Level Analysis of Mechanisms Regulating Yeast Metabolic Flux. *Science* **2016**, *354* (6311), No. aaf2786.

(55) Hu, Q.; Botuyan, M. V.; Zhao, D.; Cui, G.; Mer, E.; Mer, G. Mechanisms of BRCA1−BARD1 Nucleosome Recognition and Ubiquitylation. *Nature* **2021**, *596* (7872), 438−443.

(56) Gaur, K.; Pérez Otero, S. C.; Benjamín-Rivera, J. A.; Rodríguez, I.; Loza-Rosas, S. A.; Vázquez Salgado, A. M.; Akam, E. A.; Hernández-Matias, L.; Sharma, R. K.; Alicea, N.; Kowaleff, M.; Washington, A. V.; Astashkin, A. V.; Tomat, E.; Tinoco, A. D. Iron Chelator Transmetalative Approach to Inhibit Human Ribonucleotide Reductase. *JACS Au* **2021**, *1* (6), 865−878.

(57) Huang, J.-Q.; Fang, X.; Tian, X.; Chen, P.; Lin, J.-L.; Guo, X.-X.; Li, J.-X.; Fan, Z.; Song, W.-M.; Chen, F.-Y.; Ahati, R.; Wang, L.-J.; Zhao, Q.; Martin, C.; Chen, X.-Y. Aromatization of Natural Products by a Specialized Detoxification Enzyme. *Nat. Chem. Biol.* **2020**, *16* (3), 250−256.

(58) Semenov, S. N.; Wong, A. S. Y.; van der Made, R. M.; Postma, S. G. J.; Groen, J.; van Roekel, H. W. H.; de Greef, T. F. A.; Huck, W. T. S. Rational Design of Functional and Tunable Oscillating Enzymatic Networks. *Nat. Chem.* **2015**, *7* (2), 160−165.

(59) Zhang, W. C.; Shyh-Chang, N.; Yang, H.; Rai, A.; Umashankar, S.; Ma, S.; Soh, B. S.; Sun, L. L.; Tai, B. C.; Nga, M. E.; Bhakoo, K. K.; Jayapal, S. R.; Nichane, M.; Yu, Q.; Ahmed, D. A.; Tan, C.; Sing, W. P.; Tam, J.; Thirugananam, A.; Noghabi, M. S.; Huei Pang, Y.; Ang, H. S.; Mitchell, W.; Robson, P.; Kaldis, P.; Soo, R. A.; Swarup, S.; Lim, E. H.; Lim, B. Glycine Decarboxylase Activity Drives Non-Small Cell Lung Cancer Tumor-Initiating Cells and Tumorigenesis. *Cell* **2012**, *148* (1-2), 259−272.

(60) Hyer, M. L.; Milhollen, M. A.; Ciavarri, J.; Fleming, P.; Traore, T.; Sappal, D.; Huck, J.; Shi, J.; Gavin, J.; Brownell, J.; Yang, Y.; Stringer, B.; Griffin, R.; Bruzzese, F.; Soucy, T.; Duffy, J.; Rabino, C.; Riceberg, J.; Hoar, K.; Lublinsky, A.; Menon, S.; Sintchak, M.; Bump, N.; Pulukuri, S. M.; Langston, S.; Tirrell, S.; Kuranda, M.; Veiby, P.; Newcomb, J.; Li, P.; Wu, J. T.; Powe, J.; Dick, L. R.; Greenspan, P.; Galvin, K.; Manfredi, M.; Claiborne, C.; Amidon, B. S.; Bence, N. F. A Small-Molecule Inhibitor of the Ubiquitin Activating Enzyme for Cancer Treatment. *Nat. Med.* **2018**, *24* (2), 186−193.

(61) He, H.; Yin, J.; Li, M.; Dessai, C. V. P.; Yi, M.; Teng, X.; Zhang, M.; Li, Y.; Du, Z.; Xu, B.; Cheng, J.-X. Mapping Enzyme Activity in Living Systems by Real-Time Mid-Infrared Photothermal Imaging of Nitrile Chameleons. *Nat. Methods* **2024**, *21* (2), 342−352.

(62) Chen, Z.; Li, J.; Li, T.; Fan, T.; Meng, C.; Li, C.; Kang, J.; Chai, L.; Hao, Y.; Tang, Y.; Al-Hartomy, O. A.; Wageh, S.; Al-Sehemi, A. G.; Luo, Z.; Yu, J.; Shao, Y.; Li, D.; Feng, S.; Liu, W. J.; He, Y.; Ma, X.; Xie, Z.; Zhang, H. A CRISPR/Cas12a-Empowered Surface Plasmon Resonance Platform for Rapid and Specific Diagnosis of the Omicron Variant of SARS-CoV-2. *Natl. Sci. Rev.* **2022**, *9* (8), No. nwac104.

(63) Chen, Z.; Meng, C.; Wang, X.; Chen, J.; Deng, J.; Fan, T.; Wang, L.; Lin, H.; Huang, H.; Li, S.; Sun, S.; Qu, J.; Fan, D.; Zhang, X.; Liu, Y.; Shao, Y.; Zhang, H. Ultrasensitive DNA Origami Plasmon Sensor for Accurate Detection in Circulating Tumor DNAs. *Laser Photonics Rev.* **2024**, No. 2400035.

(64) Zheng, F.; Chen, Z.; Li, J.; Wu, R.; Zhang, B.; Nie, G.; Xie, Z.; Zhang, H. A Highly Sensitive CRISPR-Empowered Surface Plasmon Resonance Sensor for Diagnosis of Inherited Diseases with Femtomolar-Level Real-Time Quantification. *Adv. Sci.* **2022**, *9* (14), No. 2105231.

(65) Chen, Z.; Wu, C.; Yuan, Y.; Xie, Z.; Li, T.; Huang, H.; Li, S.; Deng, J.; Lin, H.; Shi, Z.; Li, C.; Hao, Y.; Tang, Y.; You, Y.; Al-Hartomy, O. A.; Wageh, S.; Al-Sehemi, A. G.; Lu, R.; Zhang, L.; Lin, X.; He, Y.; Zhao, G.; Li, D.; Zhang, H. CRISPR-Cas13a-Powered Electrochemical Biosensor for the Detection of the L452R Mutation

in Clinical Samples of SARS-CoV-2 Variants. *J. Nanobiotechnol.* **2023**, *21* (1), 141.

(66) Xue, T.; Liang, W.; Li, Y.; Sun, Y.; Xiang, Y.; Zhang, Y.; Dai, Z.; Duo, Y.; Wu, L.; Qi, K.; Shivananju, B. N.; Zhang, L.; Cui, X.; Zhang, H.; Bao, Q. Ultrasensitive Detection of miRNA with an Antimonene-Based Surface Plasmon Resonance Sensor. *Nat. Commun.* **2019**, *10* (1), 28.

(67) Zhang, Y.; Park, K.-Y.; Suazo, K. F.; Distefano, M. D. Recent Progress in Enzymatic Protein Labelling Techniques and Their Applications. *Chem. Soc. Rev.* **2018**, *47* (24), 9106−9136.

(68) Zhou, J.; Xu, B. Enzyme-Instructed Self-Assembly: A Multistep Process for Potential Cancer Therapy. *Bioconjugate Chem.* **2015**, *26* (6), 987−999.

(69) Ma, X.; Hortelão, A. C.; Patiño, T.; Sánchez, S. Enzyme Catalysis To Power Micro/Nanomachines. *ACS Nano* **2016**, *10* (10), 9111−9122.

(70) Yuan, M.; Wu, Y.; Zhao, C.; Chen, Z.; Su, L.; Yang, H.; Song, J. Activated Molecular Probes for Enzyme Recognition and Detection. *Theranostics* **2022**, *12* (3), 1459−1485.

(71) Wu, X.; Wang, R.; Kwon, N.; Ma, H.; Yoon, J. Activatable Fluorescent Probes for In Situ Imaging of Enzymes. *Chem. Soc. Rev.* **2022**, *51* (2), 450−463.

(72) Zheng, D.; Chen, Y.; Ai, S.; Zhang, R.; Gao, Z.; Liang, C.; Cao, L.; Chen, Y.; Hong, Z.; Shi, Y.; Wang, L.; Li, X.; Yang, Z. Tandem Molecular Self-Assembly Selectively Inhibits Lung Cancer Cells by Inducing Endoplasmic Reticulum Stress. *Research* **2019**, *2019*, No. 4803624.

(73) Reches, M.; Gazit, E. Casting Metal Nanowires Within Discrete Self-Assembled Peptide Nanotubes. *Science* **2003**, *300* (5619), 625−627.

(74) Rzepecki, P.; Schrader, T. β-Sheet Ligands in Action: KLVFF Recognition by Aminopyrazole Hybrid Receptors in Water. *J. Am. Chem. Soc.* **2005**, *127* (9), 3016−3025.

(75) Gao, Y.; Shi, J.; Yuan, D.; Xu, B. Imaging Enzyme-Triggered Self-Assembly of Small Molecules Inside Live Cells. *Nat. Commun.* **2012**, *3* (1), 1033.

(76) Wang, Y.; Wang, D.; Wu, C.; Wang, B.; He, S.; Wang, H.; Liang, G.; Zhang, Y. MMP 9-Instructed Assembly of bFGF Nanofibers in Ischemic Myocardium to Promote Heart Repair. *Theranostics* **2022**, *12* (17), 7237−7249.

(77) Zhao, Y.-D.; An, H.-W.; Mamuti, M.; Zeng, X.-Z.; Zheng, R.; Yang, J.; Zhou, W.; Liang, Y.; Qin, G.; Hou, D.-Y.; Liu, X.; Wang, H.; Zhao, Y.; Fang, X. Reprogramming Hypoxic Tumor-Associated Macrophages by Nanoglycoclusters for Boosted Cancer Immunotherapy. *Adv. Mater.* **2023**, *35* (24), No. 2211332.

(78) An, H.-W.; Hou, D.-Y.; Yang, J.; Wang, Z.-Q.; Wang, M.-D.; Zheng, R.; Zhang, N.-Y.; Hu, X.-J.; Wang, Z.-J.; Wang, L.; Liu, D.; Hao, J.-F.; Xu, W.; Zhao, Y.; Wang, H. A Bispecific Glycopeptide Spatiotemporally Regulates Tumor Microenvironment for Inhibiting Bladder Cancer Recurrence. *Sci. Adv.* **2023**, *9* (9), No. eabq8225.

(79) Wu, C.; Zhang, R.; Du, W.; Cheng, L.; Liang, G. Alkaline Phosphatase-Triggered Self-Assembly of Near-Infrared Nanoparticles for the Enhanced Photoacoustic Imaging of Tumors. *Nano Lett.* **2018**, *18* (12), 7749−7754.

(80) Yan, R.; Hu, Y.; Liu, F.; Wei, S.; Fang, D.; Shuhendler, A. J.; Liu, H.; Chen, H.-Y.; Ye, D. Activatable NIR Fluorescence/MRI Bimodal Probes for in Vivo Imaging by Enzyme-Mediated Fluorogenic Reaction and Self-Assembly. *J. Am. Chem. Soc.* **2019**, *141* (26), 10331−10341.

(81) Hu, Y.; Miao, Y.; Zhang, J.; Chen, Y.; Qiu, L.; Lin, J.; Ye, D. Alkaline Phosphatase Enabled Fluorogenic Reaction and in situ Coassembly of Near-Infrared and Radioactive Nanoparticles for in vivo Imaging. *Nano Lett.* **2021**, *21* (24), 10377−10385.

(82) Wen, X.; Zhang, R.; Hu, Y.; Wu, L.; Bai, H.; Song, D.; Wang, Y.; An, R.; Weng, J.; Zhang, S.; Wang, R.; Qiu, L.; Lin, J.; Gao, G.; Liu, H.; Guo, Z.; Ye, D. Controlled Sequential In Situ Self-Assembly and Disassembly of a Fluorogenic Cisplatin Prodrug for Cancer Theranostics. *Nat. Commun.* **2023**, *14* (1), 800.

(83) Wang, H.; Feng, Z.; Wang, Y.; Zhou, R.; Yang, Z.; Xu, B. Integrating Enzymatic Self-Assembly and Mitochondria Targeting for Selectively Killing Cancer Cells without Acquired Drug Resistance. *J. Am. Chem. Soc.* **2016**, *138* (49), 16046−16055.

(84) Feng, Z.; Wang, H.; Wang, S.; Zhang, Q.; Zhang, X.; Rodal, A. A.; Xu, B. Enzymatic Assemblies Disrupt the Membrane and Target Endoplasmic Reticulum for Selective Cancer Cell Death. *J. Am. Chem. Soc.* **2018**, *140* (30), 9566−9573.

(85) Tan, W.; Zhang, Q.; Wang, J.; Yi, M.; He, H.; Xu, B. Enzymatic Assemblies of Thiophosphopeptides Instantly Target Golgi Apparatus and Selectively Kill Cancer Cells. *Angew. Chem., Int. Ed.* **2021**, *60* (23), 12796−12801.

(86) Wang, Q.; Xiao, M.; Wang, D.; Hou, X.; Gao, J.; Liu, J.; Liu, J. In Situ Supramolecular Self-Assembly of Pt(IV) Prodrug to Conquer Cisplatin Resistance. *Adv. Funct. Mater.* **2021**, *31* (27), No. 2101826.

(87) Gao, G.; Sun, X.; Liu, X.; Jiang, Y.-W.; Tang, R.; Guo, Y.; Wu, F.-G.; Liang, G. Intracellular Nanoparticle Formation and Hydroxy-chloroquine Release for Autophagy-Inhibited Mild-Temperature Photothermal Therapy for Tumors. *Adv. Funct. Mater.* **2021**, *31* (34), No. 2102832.

(88) Hu, Y.; Zhang, J.; Miao, Y.; Wen, X.; Wang, J.; Sun, Y.; Chen, Y.; Lin, J.; Qiu, L.; Guo, K.; Chen, H.-Y.; Ye, D. Enzyme-Mediated In Situ Self-Assembly Promotes In Vivo Bioorthogonal Reaction for Pretargeted Multimodality Imaging. *Angew. Chem., Int. Ed.* **2021**, *60* (33), 18082−18093.

(89) Yao, Q.; Lin, F.; Fan, X.; Wang, Y.; Liu, Y.; Liu, Z.; Jiang, X.; Chen, P. R.; Gao, Y. Synergistic enzymatic and bioorthogonal reactions for selective prodrug activation in living systems. *Nat. Commun.* **2018**, *9* (1), 5032.

(90) Wen, X.; Zeng, W.; Zhang, J.; Liu, Y.; Miao, Y.; Liu, S.; Yang, Y.; Xu, J.-J.; Ye, D. Cascade In Situ Self-Assembly and Bioorthogonal Reaction Enable the Enrichment of Photosensitizers and Carbonic Anhydrase Inhibitors for Pretargeted Cancer Theranostics. *Angew. Chem., Int. Ed.* **2024**, *63* (4), No. e202314039.

(91) Hai, Z.; Ni, Y.; Saimi, D.; Yang, H.; Tong, H.; Zhong, K.; Liang, G. γ-Glutamyltranspeptidase-Triggered Intracellular Gadolinium Nanoparticle Formation Enhances the T_2-Weighted MR Contrast of Tumor. *Nano Lett.* **2019**, *19* (4), 2428−2433.

(92) Lin, J.; Gao, D.; Wang, S.; Lv, G.; Wang, X.; Lu, C.; Peng, Y.; Qiu, L. Stimuli-Responsive Macrocyclization Scaffold Allows In Situ Self-Assembly of Radioactive Tracers for Positron Emission Tomography Imaging of Enzyme Activity. *J. Am. Chem. Soc.* **2022**, *144* (17), 7667−7675.

(93) Yuan, Y.; Zhang, J.; Qi, X.; Li, S.; Liu, G.; Siddhanta, S.; Barman, I.; Song, X.; McMahon, M. T.; Bulte, J. W. M. Furin-Mediated Intracellular Self-Assembly of Olsalazine Nanoparticles for Enhanced Magnetic Resonance Imaging and Tumour Therapy. *Nat. Mater.* **2019**, *18* (12), 1376−1383.

(94) Wang, H.; Chen, P.; Wu, H.; Zou, P.; Wu, J.; Liu, Y.; Liang, G. Furin-Guided Intracellular ⁶⁸Ga Nanoparticle Formation Enhancing Tumor MicroPET Imaging. *Anal. Chem.* **2019**, *91* (23), 14842−14845.

(95) Dragulescu-Andrasi, A.; Kothapalli, S.-R.; Tikhomirov, G. A.; Rao, J.; Gambhir, S. S. Activatable Oligomerizable Imaging Agents for Photoacoustic Imaging of Furin-Like Activity in Living Subjects. *J. Am. Chem. Soc.* **2013**, *135* (30), 11015−11022.

(96) Ye, D.; Shuhendler, A. J.; Cui, L.; Tong, L.; Tee, S. S.; Tikhomirov, G.; Felsher, D. W.; Rao, J. Bioorthogonal Cyclization-Mediated In Situ Self-Assembly of Small-Molecule Probes for Imaging Caspase Activity In Vivo. *Nat. Chem.* **2014**, *6* (6), 519−526.

(97) Ye, D.; Shuhendler, A. J.; Pandit, P.; Brewer, K. D.; Tee, S. S.; Cui, L.; Tikhomirov, G.; Rutt, B.; Rao, J. Caspase-Responsive Smart Gadolinium-Based Contrast Agent for Magnetic Resonance Imaging of Drug-Induced Apoptosis. *Chem. Sci.* **2014**, *5* (10), 3845−3852.

(98) Shuhendler, A. J.; Ye, D.; Brewer, K. D.; Bazalova-Carter, M.; Lee, K.-H.; Kempen, P.; Dane Wittrup, K.; Graves, E. E.; Rutt, B.; Rao, J. Molecular Magnetic Resonance Imaging of Tumor Response to Therapy. *Sci. Rep.* **2015**, *5* (1), 14759.

(99) Nejadnik, H.; Ye, D.; Lenkov, O. D.; Donig, J. S.; Martin, J. E.; Castillo, R.; Derugin, N.; Sennino, B.; Rao, J.; Daldrup-Link, H. Magnetic Resonance Imaging of Stem Cell Apoptosis in Arthritic Joints with a Caspase Activatable Contrast Agent. *ACS Nano* **2015**, *9* (2), 1150−1160.

(100) Shen, B.; Jeon, J.; Palner, M.; Ye, D.; Shuhendler, A.; Chin, F. T.; Rao, J. Positron Emission Tomography Imaging of Drug-Induced Tumor Apoptosis with a Caspase-Triggered Nanoaggregation Probe. *Angew. Chem., Int. Ed.* **2013**, *52* (40), 10511−10514.

(101) Palner, M.; Shen, B.; Jeon, J.; Lin, J.; Chin, F. T.; Rao, J. Preclinical Kinetic Analysis of the Caspase-3/7 PET Tracer ¹⁸F-C-SNAT: Quantifying the Changes in Blood Flow and Tumor Retention After Chemotherapy. *J. Nucl. Med.* **2015**, *56* (9), 1415−1421.

(102) Witney, T. H.; Hoehne, A.; Reeves, R. E.; Ilovich, O.; Namavari, M.; Shen, B.; Chin, F. T.; Rao, J.; Gambhir, S. S. A Systematic Comparison of ¹⁸F-C-SNAT to Established Radiotracer Imaging Agents for the Detection of Tumor Response to Treatment. *Clin. Cancer Res.* **2015**, *21* (17), 3896−3905.

(103) Wang, Y.; Hu, X.; Weng, J.; Li, J.; Fan, Q.; Zhang, Y.; Ye, D. A Photoacoustic Probe for the Imaging of Tumor Apoptosis by Caspase-Mediated Macrocyclization and Self-Assembly. *Angew. Chem., Int. Ed.* **2019**, *58* (15), 4886−4890.

(104) Wang, Y.; Bai, H.; Miao, Y.; Weng, J.; Huang, Z.; Fu, J.; Zhang, Y.; Lin, J.; Ye, D. Tailoring a Near-Infrared Macrocyclization Scaffold Allows the Control of In Situ Self-Assembly for Photo-acoustic/PET Bimodal Imaging. *Angew. Chem., Int. Ed.* **2022**, *61* (14), No. e202200369.

(105) Bai, H.; Wang, Y.; Hu, Y.; Ye, D. A Caspase-3-Activatable Bimodal Probe for Photoacoustic and Magnetic Resonance Imaging of Tumor Apoptosis In Vivo. *Biosens. Bioelectron.* **2022**, *216*, No. 114648.

(106) An, H.-W.; Li, L.-L.; Wang, Y.; Wang, Z.; Hou, D.; Lin, Y.-X.; Qiao, S.-L.; Wang, M.-D.; Yang, C.; Cong, Y.; Ma, Y.; Zhao, X.-X.; Cai, Q.; Chen, W.-T.; Lu, C.-Q.; Xu, W.; Wang, H.; Zhao, Y. A Tumour-Selective Cascade Activatable Self-Detained System for Drug Delivery and Cancer Imaging. *Nat. Commun.* **2019**, *10* (1), 4861.

(107) Liu, X.; Zhan, W.; Gao, G.; Jiang, Q.; Zhang, X.; Zhang, H.; Sun, X.; Han, W.; Wu, F.-G.; Liang, G. Apoptosis-Amplified Assembly of Porphyrin Nanofiber Enhances Photodynamic Therapy of Oral Tumor. *J. Am. Chem. Soc.* **2023**, *145* (14), 7918−7930.

(108) Chen, Z.; Chen, M.; Zhou, K.; Rao, J. Pre-targeted Imaging of Protease Activity through In Situ Assembly of Nanoparticles. *Angew. Chem., Int. Ed.* **2020**, *59* (20), 7864−7870.

(109) Wang, C.; Du, W.; Wu, C.; Dan, S.; Sun, M.; Zhang, T.; Wang, B.; Yuan, Y.; Liang, G. Cathespin B-Initiated Cypate Nanoparticle Formation for Tumor Photoacoustic Imaging. *Angew. Chem., Int. Ed.* **2022**, *61* (5), No. e202114766.

(110) Dai, Q.; Xie, L.; Ren, E.; Liu, G. Cathepsin B Responsive Peptide−Purpurin Conjugates Assembly-Initiated in Situ Self-Aggregation for Cancer Sonotheranostics. *Nano Lett.* **2024**, *24* (3), 950−957.

(111) Qi, G.; Liu, X.; Shi, L.; Wu, M.; Liu, J.; Liu, B. Enzyme-Mediated Intracellular Polymerization of AIEgens for Light-Up Tumor Localization and Theranostics. *Adv. Mater.* **2022**, *34* (5), No. 2106885.

(112) Zhen, X.; Zhang, J.; Huang, J.; Xie, C.; Miao, Q.; Pu, K. Macrotheranostic Probe with Disease-Activated Near-Infrared Fluo-rescence, Photoacoustic, and Photothermal Signals for Imaging-Guided Therapy. *Angew. Chem., Int. Ed.* **2018**, *57* (26), 7804−7808.

(113) Zhao, X.-X.; Li, L.-L.; Zhao, Y.; An, H.-W.; Cai, Q.; Lang, J.-Y.; Han, X.-X.; Peng, B.; Fei, Y.; Liu, H.; Qin, H.; Nie, G.; Wang, H. In Situ Self-Assembled Nanofibers Precisely Target Cancer-Associated Fibroblasts for Improved Tumor Imaging. *Angew. Chem., Int. Ed.* **2019**, *58* (43), 15287−15294.

(114) Wang, Y.; An, R.; Luo, Z.; Ye, D. Firefly Luciferin-Inspired Biocompatible Chemistry for Protein Labeling and In Vivo Imaging. *Chem. - Eur. J.* **2018**, *24* (22), 5707−5722.

(115) Yang, Y.; Liu, X.; Wu, X.; Liang, G. Enzyme-Instructed CBT-Cys-like Click Cyclization Reactions for Bioimaging. *Chem. Biomed. Imaging* **2024**, *2* (2), 98−116.

(116) Ren, C.; Zhang, J.; Chen, M.; Yang, Z. Self-Assembling Small Molecules for the Detection of Important Analytes. *Chem. Soc. Rev.* **2014**, *43* (21), 7257−7266.

(117) Hu, B.; Song, N.; Cao, Y.; Li, M.; Liu, X.; Zhou, Z.; Shi, L.; Yu, Z. Noncanonical Amino Acids for Hypoxia-Responsive Peptide Self-Assembly and Fluorescence. *J. Am. Chem. Soc.* **2021**, *143* (34), 13854−13864.

(118) Tao, M.; Wang, M.; Jiang, C.; Liu, W.; Zhu, W.; Shi, X.; Hai, Z. Macrophage-Targeting and Hydrogen-Peroxide-Responsive Fluorescent Probe for Imaging of Inflammation In Vivo. *Chem. Biomed. Imaging* **2024**, *2* (4), 270−274.

(119) Zhang, J.; Chai, X.; He, X.-P.; Kim, H.-J.; Yoon, J.; Tian, H. Fluorogenic Probes for Disease-Relevant Enzymes. *Chem. Soc. Rev.* **2019**, *48* (2), 683−722.

(120) Yang, Z.; Liang, G.; Xu, B. Enzymatic Hydrogelation of Small Molecules. *Acc. Chem. Res.* **2008**, *41* (2), 315−326.

(121) Lee, M. H.; Kim, J. S.; Sessler, J. L. Small Molecule-Based Ratiometric Fluorescence Probes for Cations, Anions, and Biomolecules. *Chem. Soc. Rev.* **2015**, *44* (13), 4185−4191.

(122) Frederix, P. W. J. M.; Patmanidis, I.; Marrink, S. J. Molecular Simulations of Self-Assembling Bio-Inspired Supramolecular Systems and Their Connection to Experiments. *Chem. Soc. Rev.* **2018**, *47* (10), 3470−3489.

(123) Liang, G.; Ren, H.; Rao, J. A Biocompatible Condensation Reaction for Controlled Assembly of Nanostructures in Living Cells. *Nat. Chem.* **2010**, *2* (1), 54−60.

(124) Ye, D.; Liang, G.; Ma, M. L.; Rao, J. Controlling Intracellular Macrocyclization for the Imaging of Protease Activity. *Angew. Chem., Int. Ed.* **2011**, *50* (10), 2275−2279.

(125) Xie, J.; El Rami, F.; Zhou, K.; Simonetta, F.; Chen, Z.; Zheng, X.; Chen, M.; Balakrishnan, P. B.; Dai, S.-Y.; Murty, S.; Alam, I. S.; Baker, J.; Negrin, R. S.; Gambhir, S. S.; Rao, J. Multiparameter Longitudinal Imaging of Immune Cell Activity in Chimeric Antigen Receptor T Cell and Checkpoint Blockade Therapies. *ACS Cent. Sci.* **2022**, *8* (5), 590−602.

(126) Chen, Z.; Chen, M.; Cheng, Y.; Kowada, T.; Xie, J.; Zheng, X.; Rao, J. Exploring the Condensation Reaction between Aromatic Nitriles and Amino Thiols To Optimize In Situ Nanoparticle Formation for the Imaging of Proteases and Glycosidases in Cells. *Angew. Chem., Int. Ed.* **2020**, *59* (8), 3272−3279.

(127) Xiao, L.; Magupalli, V. G.; Wu, H. Cryo-EM Structures of the Active NLRP3 Inflammasome Disc. *Nature* **2023**, *613* (7944), 595−600.

(128) Xu, L.; Gao, H.; Zhan, W.; Deng, Y.; Liu, X.; Jiang, Q.; Sun, X.; Xu, J.-J.; Liang, G. Dual Aggregations of a Near-Infrared Aggregation-Induced Emission Luminogen for Enhanced Imaging of Alzheimer's Disease. *J. Am. Chem. Soc.* **2023**, *145* (50), 27748−27756.

(129) Fan, Y.; Chen, L.; Zheng, Y.; Li, A.; Lin, H.; Gao, J. Nanoparticle-Based Activatable MRI Probes for Disease Imaging and Monitoring. *Chem. Biomed. Imaging* **2023**, *1* (3), 192−204.

(130) Zhao, Z.; Li, M.; Zeng, J.; Huo, L.; Liu, K.; Wei, R.; Ni, K.; Gao, J. Recent Advances in Engineering Iron Oxide Nanoparticles for Effective Magnetic Resonance Imaging. *Bioact. Mater.* **2022**, *12*, 214−245.

(131) An, R.; Cheng, X.; Wei, S.; Hu, Y.; Sun, Y.; Huang, Z.; Chen, H.-Y.; Ye, D. Smart Magnetic and Fluorogenic Photosensitizer Nanoassemblies Enable Redox-Driven Disassembly for Photodynamic Therapy. *Angew. Chem., Int. Ed.* **2020**, *59* (46), 20636−20644.

(132) Li, H.; Hai, Z.; Zou, L.; Zhang, L.; Wang, L.; Wang, L.; Liang, G. Simultaneous Enhancement of T_1 and T_2 Magnetic Resonance Imaging of Liver Tumor at Respective Low and High Magnetic Fields. *Theranostics* **2022**, *12* (1), 410−417.

(133) Alipour, A.; Soran-Erdem, Z.; Utkur, M.; Sharma, V. K.; Algin, O.; Saritas, E. U.; Demir, H. V. A New Class of Cubic SPIONs as a Dual-Mode T_1 and T_2 Contrast Agent for MRI. *Magn. Reson. Imaging* **2018**, *49*, 16−24.

(134) Kievit, F. M.; Zhang, M. Surface Engineering of Iron Oxide Nanoparticles for Targeted Cancer Therapy. *Acc. Chem. Res.* **2011**, *44* (10), 853−862.

(135) Barrow, M.; Taylor, A.; Murray, P.; Rosseinsky, M. J.; Adams, D. J. Design Considerations for the Synthesis of Polymer Coated Iron Oxide Nanoparticles for Stem Cell Labelling and Tracking Using MRI. *Chem. Soc. Rev.* **2015**, *44* (19), 6733−6748.

(136) Iyad, N.; Ahmad, M. S.; Alkhatib, S. G.; Hjouj, M. Gadolinium Contrast Agents Challenges and Opportunities of a Multidisciplinary Approach: Literature Review. *Eur. J. Radiol. Open* **2023**, *11*, No. 100503.

(137) Ali, M. M.; Liu, G.; Shah, T.; Flask, C. A.; Pagel, M. D. Using Two Chemical Exchange Saturation Transfer Magnetic Resonance Imaging Contrast Agents for Molecular Imaging Studies. *Acc. Chem. Res.* **2009**, *42* (7), 915−924.

(138) Rao, J. Imaging of Tumour Acidosis with PET. *Nat. Biomed. Eng.* **2020**, *4* (3), 250−251.

(139) Schwenck, J.; Sonanini, D.; Cotton, J. M.; Rammensee, H.-G.; la Fougère, C.; Zender, L.; Pichler, B. J. Advances in PET Imaging of Cancer. *Nat. Rev. Cancer* **2023**, *23* (7), 474−490.

(140) Gawne, P. J.; Man, F.; Blower, P. J.; T. M. de Rosales, R. Direct Cell Radiolabeling for in Vivo Cell Tracking with PET and SPECT Imaging. *Chem. Rev.* **2022**, *122* (11), 10266−10318.

(141) Liu, Y.; Teng, L.; Yin, B.; Meng, H.; Yin, X.; Huan, S.; Song, G.; Zhang, X.-B. Chemical Design of Activatable Photoacoustic Probes for Precise Biomedical Applications. *Chem. Rev.* **2022**, *122* (6), 6850−6918.

(142) Chen, G.; Qiu, H.; Prasad, P. N.; Chen, X. Upconversion Nanoparticles: Design, Nanochemistry, and Applications in Theranostics. *Chem. Rev.* **2014**, *114* (10), 5161−5214.

(143) Zhang, X.; Wu, Y.; Chen, L.; Song, J.; Yang, H. Optical and Photoacoustic Imaging In Vivo: Opportunities and Challenges. *Chem. Biomed. Imaging* **2023**, *1* (2), 99−109.

(144) Le-Vinh, B.; Akkuş-Dağdeviren, Z. B.; Le, N.-M. N.; Nazir, I.; Bernkop-Schnürch, A. Alkaline Phosphatase: A Reliable Endogenous Partner for Drug Delivery and Diagnostics. *Adv. Ther.* **2022**, *5* (2), No. 2100219.

(145) Wang, Y.; Hu, Y.; Ye, D. Activatable Multimodal Probes for In Vivo Imaging and Theranostics. *Angew. Chem., Int. Ed.* **2022**, *61* (50), No. e202209512.

(146) Li, B.; Pang, E.; Zhao, S.; Deng, G.; Wang, S.; Wang, B.; Wu, J.; Niu, G.; Song, X.; Lan, M. Aggregation-Enhanced Photophysical Performance of D-π-A Structured Hemicyanine for NIR-II Fluorescent and Photoacoustic Imaging-Guided Photothermal Therapy. *Chem. Biomed. Imaging* **2023**, *1* (6), 541−549.

(147) He, S.; Song, J.; Qu, J.; Cheng, Z. Crucial Breakthrough of Second Near-Infrared Biological Window Fluorophores: Design and Synthesis Toward Multimodal Imaging and Theranostics. *Chem. Soc. Rev.* **2018**, *47* (12), 4258−4278.

(148) Sun, Y.; Ma, X.; Cheng, K.; Wu, B.; Duan, J.; Chen, H.; Bu, L.; Zhang, R.; Hu, X.; Deng, Z.; Xing, L.; Hong, X.; Cheng, Z. Strained Cyclooctyne as a Molecular Platform for Construction of Multimodal Imaging Probes. *Angew. Chem., Int. Ed.* **2015**, *54* (20), 5981−5984.

(149) Li, C.; Penet, M.-F.; Wildes, F.; Takagi, T.; Chen, Z.; Winnard, P. T., Jr.; Artemov, D.; Bhujwalla, Z. M. Nanoplex Delivery of siRNA and Prodrug Enzyme for Multimodality Image-Guided Molecular Pathway Targeted Cancer Therapy. *ACS Nano* **2010**, *4* (11), 6707−6716.

(150) Debroye, E.; Parac-Vogt, T. N. Towards polymetallic Lanthanide Complexes as Dual Contrast Agents for Magnetic Resonance and Optical Imaging. *Chem. Soc. Rev.* **2014**, *43* (23), 8178−8192.

(151) Kasten, B. B.; Jiang, K.; Cole, D.; Jani, A.; Udayakumar, N.; Gillespie, G. Y.; Lu, G.; Dai, T.; Rosenthal, E. L.; Markert, J. M.; Rao, J.; Warram, J. M. Targeting MMP-14 for Dual PET and Fluorescence Imaging of Glioma in Preclinical Models. *Eur. J. Nucl. Med. Mol. Imaging* **2020**, *47* (6), 1412−1426.

(152) Sim, N.; Parker, D. Critical Design Issues in the Targeted Molecular Imaging of Cell Surface Receptors. *Chem. Soc. Rev.* **2015**, *44* (8), 2122−2134.

(153) Yin, P.; Li, D.; Liu, T. Solution Behaviors and Self-Assembly of Polyoxometalates as Models of Macroions and Amphiphilic Polyoxometalate−Organic Hybrids as Novel Surfactants. *Chem. Soc. Rev.* **2012**, *41* (22), 7368−7383.

(154) Steinberg, I.; Huland, D. M.; Vermesh, O.; Frostig, H. E.; Tummers, W. S.; Gambhir, S. S. Photoacoustic Clinical Imaging. *Photoacoustics* **2019**, *14*, 77−98.

(155) Bardhan, R.; Lal, S.; Joshi, A.; Halas, N. J. Theranostic Nanoshells: From Probe Design to Imaging and Treatment of Cancer. *Acc. Chem. Res.* **2011**, *44* (10), 936−946.

(156) Cheng, H.-B.; Cao, X.; Zhang, S.; Zhang, K.; Cheng, Y.; Wang, J.; Zhao, J.; Zhou, L.; Liang, X.-J.; Yoon, J. BODIPY as a Multifunctional Theranostic Reagent in Biomedicine: Self-Assembly, Properties, and Applications. *Adv. Mater.* **2023**, *35* (18), No. 2207546.

(157) Ghosh, S.; Lee, S. J.; Hsu, J. C.; Chakraborty, S.; Chakravarty, R.; Cai, W. Cancer Brachytherapy at the Nanoscale: An Emerging Paradigm. *Chem. Biomed. Imaging* **2024**, *2* (1), 4−26.

(158) Hutchinson, L. Killing Vessels Improves Delivery. *Nat. Rev. Clin. Oncol.* **2011**, *8* (2), 63−63.

(159) Gasparini, G.; Longo, R.; Toi, M.; Ferrara, N. Angiogenic Inhibitors: a New Therapeutic Strategy in Oncology. *Nat. Clin. Pract. Oncol.* **2005**, *2* (11), 562−577.

(160) Marrache, S.; Pathak, R. K.; Dhar, S. Detouring of Cisplatin to Access Mitochondrial Genome for Overcoming Resistance. *Proc. Natl. Acad. Sci. U. S. A.* **2014**, *111* (29), 10444−10449.

(161) Li, X.; Lovell, J. F.; Yoon, J.; Chen, X. Clinical Development and Potential of Photothermal and Photodynamic Therapies for Cancer. *Nat. Rev. Clin. Oncol.* **2020**, *17* (11), 657−674.

(162) Xu, C.; Pu, K. Second Near-Infrared Photothermal Materials For Combinational Nanotheranostics. *Chem. Soc. Rev.* **2021**, *50* (2), 1111−1137.

(163) Yu, Q.; Zhou, J.; Wang, H.; Liu, Y.; Zhou, H.; Kang, B.; Chen, H.-Y.; Xu, J.-J. A Multiple-Response Cascade Nanoreactor for Starvation and Deep Catalysis Chemodynamic Assisted Near-Infrared-II Mild Photothermal Therapy. *Chem. Biomed. Imaging* **2023**, *1* (3), 242−250.

(164) Son, S.; Kim, J. H.; Wang, X.; Zhang, C.; Yoon, S. A.; Shin, J.; Sharma, A.; Lee, M. H.; Cheng, L.; Wu, J.; Kim, J. S. Multifunctional Sonosensitizers in Sonodynamic Cancer Therapy. *Chem. Soc. Rev.* **2020**, *49* (11), 3244−3261.

(165) Zhang, D.; Qi, G.-B.; Zhao, Y.-X.; Qiao, S.-L.; Yang, C.; Wang, H. In Situ Formation of Nanofibers from Purpurin18-Peptide Conjugates and the Assembly Induced Retention Effect in Tumor Sites. *Adv. Mater.* **2015**, *27* (40), 6125−6130.

(166) An, R.; Liu, L.; Wei, S.; Huang, Z.; Qiu, L.; Lin, J.; Liu, H.; Ye, D. Controlling Disassembly of Paramagnetic Prodrug and Photo-sensitizer Nanoassemblies for On-Demand Orthotopic Glioma Theranostics. *ACS Nano* **2022**, *16* (12), 20607−20621.

(167) Liu, L.; Zhang, J.; An, R.; Xue, Q.; Cheng, X.; Hu, Y.; Huang, Z.; Wu, L.; Zeng, W.; Miao, Y.; Li, J.; Zhou, Y.; Chen, H.-Y.; Liu, H.; Ye, D. Smart Nanosensitizers for Activatable Sono-Photodynamic Immunotherapy of Tumors by Redox-Controlled Disassembly. *Angew. Chem., Int. Ed.* **2023**, *62* (10), No. e202217055.

(168) Liang, J.-L.; Luo, G.-F.; Chen, W.-H.; Zhang, X.-Z. Recent Advances in Engineered Materials for Immunotherapy-Involved Combination Cancer Therapy. *Adv. Mater.* **2021**, *33* (31), No. 2007630.

(169) Zhan, W.; Xu, L.; Liu, Z.; Liu, X.; Gao, G.; Xia, T.; Cheng, X.; Sun, X.; Wu, F.-G.; Yu, Q.; Liang, G. Tandem Guest-Host-Receptor Recognitions Precisely Guide Ciprofloxacin to Eliminate Intracellular Staphylococcus aureus. *Angew. Chem., Int. Ed.* **2023**, *62* (32), No. e202306427.

(170) Zhou, Q.; Si, Z.; Wang, K.; Li, K.; Hong, W.; Zhang, Y.; Li, P. Enzyme-triggered smart antimicrobial drug release systems against bacterial infections. *J. Controlled Release* **2022**, *352*, 507−526.

(171) Huang, Z.; Hu, Y.; Yang, Y.; Huang, W.; Wang, Y.; Ye, D. Recent Advances in Pretargeted Imaging of Tumors in Vivo. *Anal. Sensing* **2022**, *2* (4), No. e202200013.

(172) Liu, G. A Revisit to the Pretargeting Concept—A Target Conversion. *Front. Pharmacol.* **2018**, *9*, 1476.

(173) Yang, J.; Zhu, B.; Ran, C. The Application of Bio-orthogonality for In Vivo Animal Imaging. *Chem. Biomed. Imaging* **2023**, *1* (5), 434−447.

(174) Valencia-Hernandez, A. M.; Ng, W. Y.; Ghazanfari, N.; Ghilas, S.; de Menezes, M. N.; Holz, L. E.; Huang, C.; English, K.; Naung, M.; Tan, P. S.; Tullett, K. M.; Steiner, T. M.; Enders, M. H.; Beattie, L.; Chua, Y. C.; Jones, C. M.; Cozijnsen, A.; Mollard, V.; Cai, Y.; Bowen, D. G.; Purcell, A. W.; La Gruta, N. L.; Villadangos, J. A.; de Koning-Ward, T.; Barry, A. E.; Barchet, W.; Cockburn, I. A.; McFadden, G. I.; Gras, S.; Lahoud, M. H.; Bertolino, P.; Schittenhelm, R. B.; Caminschi, I.; Heath, W. R.; Fernandez-Ruiz, D. A Natural Peptide Antigen within the Plasmodium Ribosomal Protein RPL6 Confers Liver T_{RM} Cell-Mediated Immunity against Malaria in Mice. *Cell Host Microbe* **2020**, *27* (6), 950−962.

(175) Leko, V.; Rosenberg, S. A. Identifying and Targeting Human Tumor Antigens for T Cell-Based Immunotherapy of Solid Tumors. *Cancer Cell* **2020**, *38* (4), 454−472.

(176) Pazoki, R.; Vujkovic, M.; Elliott, J.; Evangelou, E.; Gill, D.; Ghanbari, M.; van der Most, P. J.; Pinto, R. C.; Wielscher, M.; Farlik, M.; Zuber, V.; de Knegt, R. J.; Snieder, H.; Uitterlinden, A. G.; Boezen, H. M.; Franke, L.; van der Harst, P.; Navis, G.; Rots, M.; Swertz, M.; Wolffenbuttel, B. H. R.; Wijmenga, C.; Lynch, J. A.; Jiang, X.; Said, S.; Kaplan, D. E.; Lee, K. M.; Serper, M.; Carr, R. M.; Tsao, P. S.; Atkinson, S. R.; Dehghan, A.; Tzoulaki, I.; Ikram, M. A.; Herzig, K.-H.; Järvelin, M.-R.; Alizadeh, B. Z.; O'Donnell, C. J.; Saleheen, D.; Voight, B. F.; Chang, K.-M.; Thursz, M. R.; Elliott, P.; Ballas, Z. K.; Bhushan, S.; Boyko, E. J.; Cohen, D. M.; Concato, J.; Aslan, M.; Zhao, H.; Constans, J. I.; Dellitalia, L. J.; Fayad, J. M.; Fernando, R. S.; Florez, H. J.; Gaddy, M. A.; Gappy, S. S.; Gibson, G.; Godschalk, M.; Greco, J. A.; Gupta, S.; Gutierrez, S.; Hammer, K. D.; Hamner, M. B.; Harley, J. B.; Hung, A. M.; Huq, M.; Hurley, R. A.; Iruvanti, P. R.; Ivins, D. J.; Jacono, F. J.; Jhala, D. N.; Kaminsky, L. S.; Klein, J. B.; Liangpunsakul, S.; Lichy, J. H.; Moser, J.; Huang, G. D.; Muralidhar, S.; Mastorides, S. M.; Mathew, R. O.; Mattocks, K. M.; McArdle, R.; Meyer, P. N.; Meyer, L. J.; Moorman, J. P.; Morgan, T. R.; Murdoch, M.; Okusaga, O. O.; Oursler, K.-A. K.; Ratcliffe, N. R.; Rauchman, M. I.; Robey, R. B.; Ross, G. W.; Servatius, R. J.; Sharma, S. C.; Sherman, S. E.; Sonel, E.; Sriram, P.; Stapley, T.; Striker, R. T.; Tandon, N.; Villareal, G.; Wallbom, A. S.; Wells, J. M.; Whittle, J. C.; Whooley, M. A.; Wilson, P. W.; Sun, Y. V.; Xu, J.; Yeh, S.-S.; Connor, T.; Argyres, D. P.; Hauser, E. R.; Beckham, J. C.; Stephens, B.; Aguayo, S. M.; Ahuja, S. K.; Pyarajan, S.; Cho, K.; Gaziano, J. M.; Kinlay, S.; Nguyen, X.-M. T.; Brewer, J. V.; Brophy, M. T.; Do, N. V.; Humphries, D. E.; Selva, L. E.; Shayan, S.; Whitbourne, S. B.; Breeling, J. L.; Romero, J. P. C.; Ramoni, R. B. Genetic Analysis in European Ancestry Individuals Identifies 517 Loci Associated with Liver Enzymes. *Nat. Commun.* **2021**, *12* (1), 2579.

(177) Wei, Y.; Song, S.; Duan, N.; Wang, F.; Wang, Y.; Yang, Y.; Peng, C.; Li, J.; Nie, D.; Zhang, X.; Guo, S.; Zhu, C.; Yu, M.; Gan, Y. MT1-MMP-Activated Liposomes to Improve Tumor Blood Perfusion and Drug Delivery for Enhanced Pancreatic Cancer Therapy. *Adv. Sci.* **2020**, *7* (17), No. 1902746.

(178) Hu, Y.; Yu, J.; Xu, M.; Pu, K. Bienzyme-Locked Activatable Fluorescent Probes for Specific Imaging of Tumor-Associated Mast Cells. *J. Am. Chem. Soc.* **2024**, *146* (18), 12656−12663.

(179) Fantoni, N. Z.; El-Sagheer, A. H.; Brown, T. A Hitchhiker's Guide to Click-Chemistry with Nucleic Acids. *Chem. Rev.* **2021**, *121* (12), 7122−7154.

(180) Wu, S.; Yue, P.; Ma, Y.; Zou, Y.; Liang, W.; Ye, Q. Hemoperfusion Adsorbents for Removal of Common Toxins in Liver and Kidney Failure: Recent Progress, Challenges, and Prospects. *Adv. Mater.* **2023**, DOI: 10.1002/adma.202305152.

(181) Dolgin, E. Radioactive drugs emerge from the shadows to storm the market. *Nat. Biotechnol.* **2018**, *36* (12), 1125−1127.

(182) Garland, K. M.; Sheehy, T. L.; Wilson, J. T. Chemical and Biomolecular Strategies for STING Pathway Activation in Cancer Immunotherapy. *Chem. Rev.* **2022**, *122* (6), 5977−6039.

(183) Li, X.; Wang, X.; Ito, A. Tailoring Inorganic Nanoadjuvants Towards Next-Generation Vaccines. *Chem. Soc. Rev.* **2018**, *47* (13), 4954−4980.

(184) He, S.; Cheng, P.; Pu, K. Activatable Near-Infrared Probes for The Detection of Specific Populations of Tumour-Infiltrating Leukocytes in Vivo and in Urine. *Nat. Biomed. Eng.* **2023**, *7* (3), 281−297.